AGU PUBLICATIONS

JGR

Journal of Geophysical Research: Earth Surface

RESEARCH ARTICLE

10.1002/2013JF002919

Key Points:
- Hillslope gradients in central Andes increase with increasing vegetation cover
- Precipitation intensity affects topography most in densely vegetated areas
- Mean annual precipitation affects erosional efficiency through vegetation cover

Supporting Information:
- Readme
- Table S1
- Table S2
- Table S3
- Table S4
- Table S5
- Table S6
- Table S7
- Table S8

Correspondence to:
M. L. Jeffery,
louise.jeffery@pik-potsdam.de

Citation:
Jeffery, M. L., B. J. Yanites, C. J. Poulsen, and T. A. Ehlers (2014), Vegetation-precipitation controls on Central Andean topography, *J. Geophys. Res. Earth Surf.*, *119*, 1354–1375, doi:10.1002/2013JF002919.

Received 14 JUL 2013
Accepted 30 APR 2014
Accepted article online 5 MAY 2014
Published online 26 JUN 2014

Vegetation-precipitation controls on Central Andean topography

M. Louise Jeffery[1,2], Brian J. Yanites[1,3], Christopher J. Poulsen[1], and Todd A. Ehlers[4,1]

[1]Department of Earth and Environmental Sciences, University of Michigan, Ann Arbor, Michigan, USA, [2]Now at Potsdam Institute for Climate Impact Research, Potsdam, Germany, [3]Now at Department of Geological Sciences, University of Idaho, Moscow, Idaho, USA, [4]Department of Geosciences, Universität Tübingen, Germany

Abstract Climatic controls on fluvial landscapes are commonly characterized in terms of mean annual precipitation. However, physical erosion processes are driven by extreme events and are therefore more directly related to the intensity, duration, and frequency of individual rainfall events. Climate also influences erosional processes indirectly by controlling vegetation. In this study, we explore how interdependent climate and vegetation properties affect landscape morphology at the scale of the Andean orogen. The mean intensity, duration, and frequency of precipitation events are derived from the TRMM 3B42v7 product. Relationships between mean hillslope gradients and precipitation event metrics, mean annual precipitation, vegetation, and bedrock lithology in the central Andes are examined by correlation analyses and multiple linear regression. Our results indicate that mean hillslope gradient correlates most strongly with percent vegetation cover ($r = 0.56$). Where vegetation cover is less than 95%, mean hillslope gradients increase with mean annual precipitation ($r = 0.60$) and vegetation cover ($r = 0.69$). Where vegetation cover is dense (>95%), mean hillslope gradients increase with increasing elevation ($r = 0.74$), decreasing inter-storm duration ($r = -0.69$), and decreasing precipitation intensity by ~0.5°/(mm d^{-1}) ($r = -0.56$). Thus, we conclude that at the orogen scale, climate influences on topography are mediated by vegetation, which itself is dependent on mean annual precipitation ($r = 0.77$). Observations from the central Andes are consistent with landscape evolution models in which hillslope gradients are a balance between rock uplift, climatic erosional efficiency and erosional resistance of the landscape determined by bedrock lithology and vegetation.

1. Introduction

Climate and vegetation have long been recognized as major interdependent controls on surface processes [e.g., *Abrahams and Ponczynski*, 1984; *Istanbulluoglu and Bras*, 2005; *Langbein and Schumm*, 1958; *Tucker and Slingerland*, 1997]. Precipitation facilitates the removal and transport of sediment from hillslopes to basins by physical processes, including rain splash, surface runoff, increased ground saturation, and fluvial incision. Vegetation can counteract the erosional capacity of precipitation by, for example, providing resistance against downslope processes through root cohesion [*Roering et al.*, 2003] and obstruction of surface flow [*Wainwright et al.*, 2000]. As climate and vegetation are not independent, distinguishing robust signals of these two factors in topography and the distribution of erosion has proved challenging [*Whipple*, 2009]. Unraveling these interdependent controls is further complicated by the dependence of climate on large-scale topography [*Kutzbach et al.*, 1989], such as the influence of the Andes on South American climate [*Insel et al.*, 2010a; *Jeffery et al.*, 2012; *Lenters and Cook*, 1997]. In this study, we use satellite observations to explore interdependent relationships among climate, vegetation, and topography characteristics in the central Andes with a focus on identifying the important characteristics of precipitation and vegetation.

Climatic erosional efficiency, that is, the potential for climatic properties to drive erosion, is commonly characterized using long-term mean observations, such as mean annual precipitation (MAP) [*Champagnac et al.*, 2012; *Montgomery et al.*, 2001]. However, climatic erosional efficiency may be more usefully described in terms of the variability, or storminess, of precipitation events [*Collins and Bras*, 2010; *Collins et al.*, 2004; *Dadson et al.*, 2003; *Eagleson*, 1978; *Lague et al.*, 2005; *Molnar et al.*, 2006; *Tucker and Bras*, 2000]. The intensity of precipitation is particularly important for geomorphic processes that require a critical erosion threshold to be exceeded [*Dietrich et al.*, 1992; *Lague et al.*, 2005; *Montgomery and Dietrich*, 1992; *Tucker*, 2004]. Intense, long-duration precipitation events are more likely than low-intensity, short-duration events to exceed infiltration capacities and cause surface runoff that can detach and transport sediment. In other settings,

landslides can be triggered by changes in stress regime through water saturation of surface material during long-duration, high-intensity precipitation events. Vegetation cover can serve as a local control on erosion [*Collins and Bras*, 2010; *Collins et al*., 2004; *Istanbulluoglu and Bras*, 2005] by increasing cohesion through root strengthening and modifying surface roughness, thereby changing the energy required to move sediment [*Hales et al*., 2009; *Schmidt et al*., 2001; *Wainwright et al*., 2000]. In addition, vegetation can reduce the erosion potential of rainfall by providing leaf litter ground cover, intercepting rainfall in the canopy, and increasing soil infiltration capacity [*Wainwright et al*., 2000]. Conversely, vegetation may also help to enhance erosion by redistributing the soil, e.g., tree-fall, and enhancing chemical weathering.

The effects of climate and vegetation on fluvial landscape morphology have been explored through both modeling and field studies. Landscape evolution models (LEMs) predict that in stormier climates, fluvial landscapes will have lower relief, lower slopes, and higher drainage density (Figure 1c) [*Tucker*, 2004; *Tucker and Slingerland*, 1997; *Tucker and Bras*, 2000]. In contrast, dense vegetation cover is found to promote higher hillslope gradients, higher relief, and lower drainage density (Figure 1d) [*Collins et al*., 2004; *Istanbulluoglu and Bras*, 2005; *Wainwright et al*., 2000]. Observational studies of relationships between sediment yield and topographic properties, such as drainage density and relief, have been performed in a range of climatic and vegetation settings. For sites in the U.S., *Langbein and Schumm* [1958] demonstrated that sediment yield increases with MAP until grassland vegetation is established. However, further increases in MAP lead to a decrease in sediment yield until the establishment of woodland forest, for which there is no direct relationship. Relationships between topographic characteristics or sediment yields and both mean annual precipitation [*Abrahams*, 1972; *Daniel*, 1981; *Melton*, 1957] and precipitation intensity [*Abrahams*, 1972; *Abrahams and Ponczynski*, 1984; *Chorley and Morgan*, 1962; *Cotton*, 1964; *Musgrave*, 1947] have been examined in a wide range of global settings. In the Bolivian Andes, sediment yields correlate with hillslope gradient and bedrock lithology but not modern river discharge [*Aalto et al*., 2006]. In the same region, erosion rates on longer (cosmogenic radionuclide, CRN) timescales do not correlate with either climatic or topographic variables [*Insel et al*., 2010b]. However, further south in the Argentinian central Andes, *Bookhagen and Strecker* [2012] showed that erosion rates on CRN timescales correspond strongly with the steep precipitation gradient. The impact of climate on landforms and erosion rates in the central Andes therefore remains unresolved.

In this study, we take advantage of recent advances in satellite-based observations to examine the influence of more complex precipitation characteristics and vegetation on topographic properties at the scale of a mountain belt. Satellite-based precipitation observations now enable examination of precipitation characteristics, such as the intensity, duration, and frequency of precipitation events, in a broader range of climatic and tectonic settings. Furthermore, remotely sensed vegetation and topography data sets are now available in the same regions. In this study, we jointly analyze these data sets to explore the relative importance of the mean climate state, precipitation variability, and vegetation in determining topographic characteristics in the tectonically active central Andes. More specifically, we address whether modern topography more strongly reflects mean annual precipitation, precipitation intensity, or vegetation characteristics (Figure 1f). The analysis is performed in the central Andes for two reasons: (1) the central Andes are characterized by large climatic gradients and (2) TRMM observations have a high quality at lower latitudes ($<35°$). This analysis also contributes to ongoing research examining unresolved relationships between erosion processes and climate over different timescales in this region [*Aalto et al*., 2006; *Bookhagen and Strecker*, 2012; *Insel et al*., 2010b; *Jeffery et al*., 2013; *McQuarrie et al*., 2008; *Montgomery et al*., 2001].

2. Data and Methods

2.1. Topographic Data

The central Andes (10–30°S) are separated by drainage divides into three separate geographic regions: the western flank, the eastern flank, and the internally drained Altiplano (Figure 2a). We distinguish these three regions because they represent regions with distinct climate, large-scale topography, and broad lithological composition (see section 2.4 below). The western flank is a crustal-scale monocline with minor surface breaking faults and block uplift of the coastal region [*Farias et al*., 2005; *Isacks*, 1988; *Schildgen et al*., 2009]. At the surface, this structure is expressed as a relatively smooth ramp extending from the western Cordillera to the Pacific

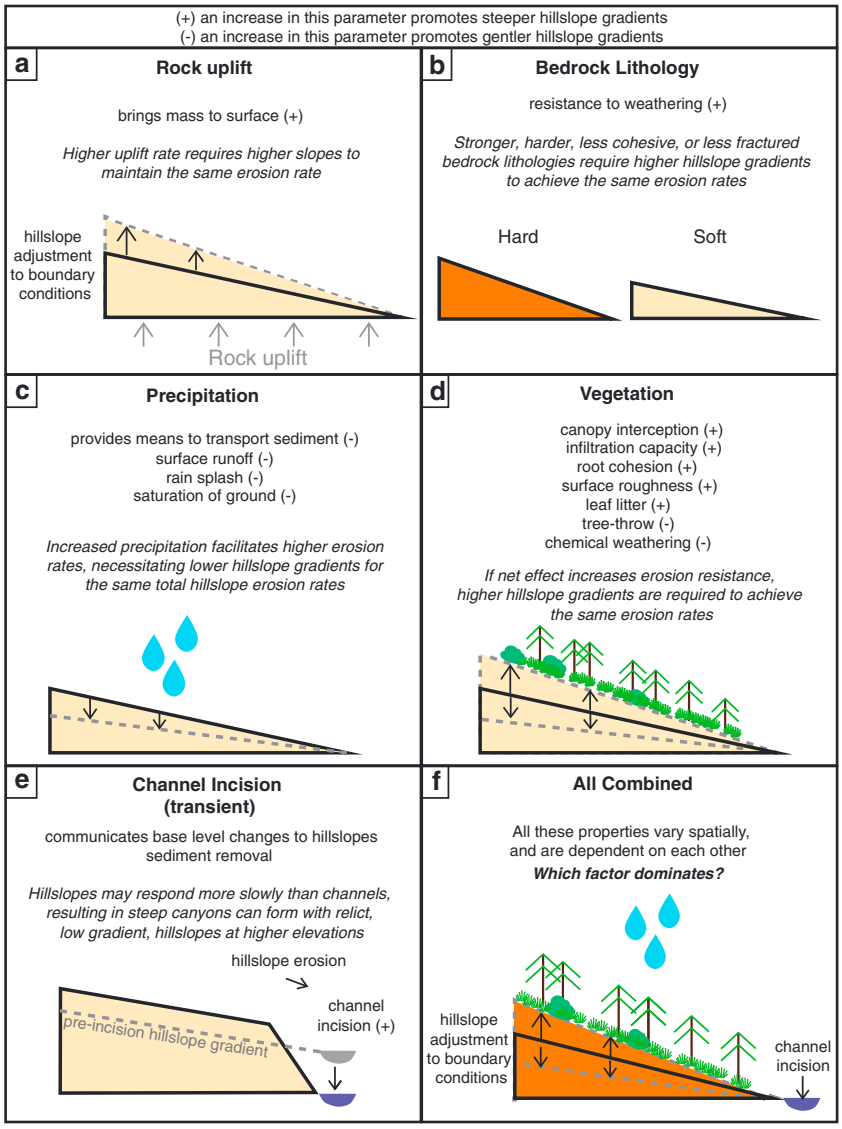

Figure 1. Hillslope gradients are determined by and respond to changes in boundary conditions. Factors that may affect hillslope gradients include (a) uplift rates, (b) bedrock lithology, (c) precipitation, (d) vegetation, and (e) transient conditions driven by changes in channel incision rates. Bedrock lithology, precipitation, and vegetation are predicted to affect hillslope gradients by modifying the erosion resistance of the surface, the erosion potential of the climate, or both [*Istanbulluoglu and Bras*, 2005; *Wainwright et al.*, 2000]. Uplift and channel incision modify the local and regional base level, with channel incision rates being more important during transient than equilibrium conditions. (f) Hillslope responses to individual factors have been observed at the catchment scale and simulated in landscape evolution models, but the relative importance of different factors at the orogen scale is not fully constrained.

Coast and dissected by deeply incised canyons. In contrast, the eastern flank is a fold and thrust belt [e.g., *Allmendinger et al.*, 1997] with a surface expression of ridges and valleys dissected along strike by large drainage networks. The consensus view is that deformation of the eastern Andean flank has migrated eastward from the Eastern Cordillera (~40–22 Ma) to the Interandean zone (by ~20–15 Ma) and the Subandes (~15–10 Ma) [*Barnes and Ehlers*, 2009]. The Altiplano is predominantly a depositional basin with localized inverted basins. The highest relief is at the basin margins in the western and eastern Cordilleras and locally at Quaternary volcanoes.

Precipitation and vegetation patterns are compared with topographic metrics derived from the 90 m Shuttle Radar Topography Mission v3 DEM [*Farr et al.*, 2007]. This study primarily focuses on the controls on mean hillslope gradient. We calculate the hillslope gradient for each grid cell in ArcGIS as the maximum change in elevation between neighboring cells in the local 3×3 grid. To make direct comparisons, elevation and

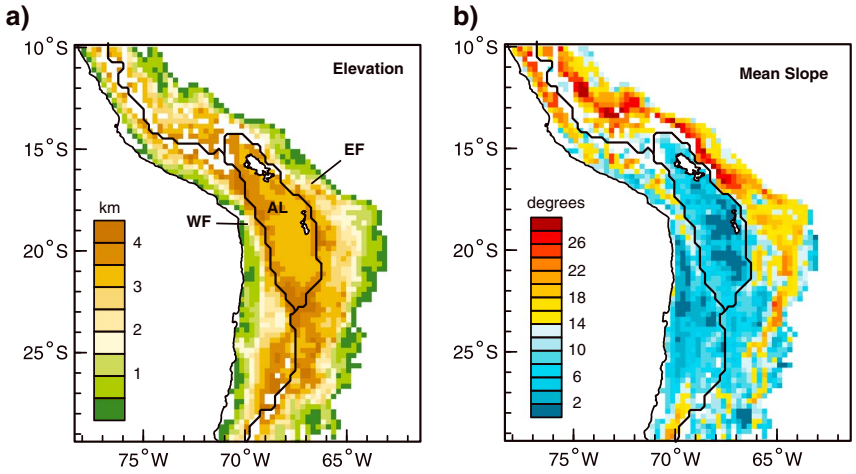

Figure 2. Surface properties regridded to the TRMM precipitation grid (Figure 4). (a) Mean surface elevation (km) and (b) mean surface slope (deg) derived from 90 m SRTM data. Only grid cells with an average elevation of >600 m and that were less than 40% glaciated at the LGM are shown. Regions described in the main text are indicated as WF, western flanks; AL, Altiplano; and EF, eastern flanks. Altiplano lakes (Titicaca and Poopó) are outlined in black for spatial reference.

hillslope gradients are regridded to match the coarser resolution precipitation data (0.25°, or ~27 km, see section 2.2) by spatial averaging (Figures 2a and 2b). The mean of the topographic data is calculated for each grid cell of the lower resolution TRMM data set. For a subsample of the region, the distribution of hillslope gradients within each coarser grid cell was analyzed. Within each coarser grid cell, hillslope gradients generally followed a normal distribution. The skewness of the distributions was low, indicating that the mean hillslope gradient within each coarse grid cell is a good representation of hillslope gradients within that grid cell. In low gradient (<5°) regions, hillslope gradients have an exponential distribution skewed toward flat surfaces (0°).

2.2. Precipitation Data

Spatial maps of precipitation are derived from NASA's Tropical Rainfall Measuring Mission (TRMM) 3B42v7 product. TRMM 3B42v7 is a 3-hourly, 0.25° × 0.25° precipitation rate data set that was derived by merging precipitation radar, infrared (IR), and microwave observations from multiple satellites, including the TRMM satellite [*Huffman et al.*, 2007]. Precipitation radar and microwave observations are used to calibrate IR observations. The product is then further calibrated using monthly GPCP rain gauge observations. TRMM 3B42v7 was chosen from the available precipitation data sets over South America because it has the highest spatial resolution with a temporal resolution that was sufficient to calculate precipitation intensity. Precipitation in the TRMM data set is rainfall only; throughout this paper, precipitation therefore refers to rainfall only and does not include snowfall. We considered using reanalysis products (e.g., NCEP-NCAR and CFSR) for their high temporal resolution, but upon evaluation of these products, we determined that

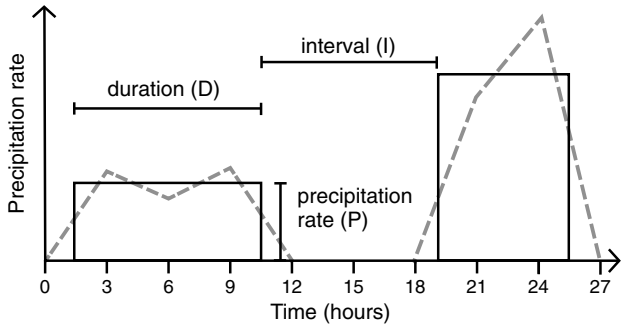

Figure 3. Precipitation metrics are defined after *Eagleson* [1978] and *Tucker and Bras* [2000] as follows. Each precipitation event (dashed lines) is approximated as a rectangular pulse (solid lines) that is described by (1) precipitation rate (P) that is the mean of all instantaneous observations during that event, (2) duration of the event (D), and (3) the interval (I) before the next event begins. At each grid point in the TRMM data set, all precipitation events are extracted from the time series. The mean of these three metrics (P, D, and I) is then calculated over all events, at each grid point, to give $\overline{P}$, $\overline{D}$, and $\overline{I}$ (Figure 4). Mean annual precipitation (MAP) is calculated independently as the total precipitation at each grid point divided by the number of years of observation.

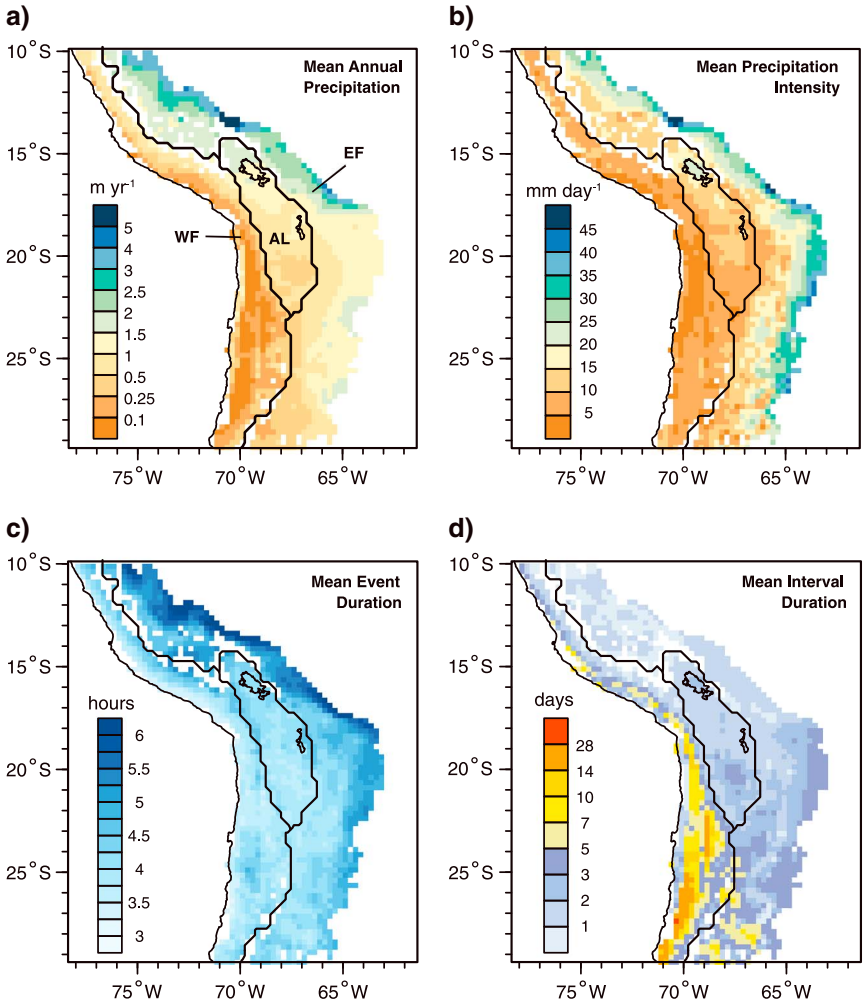

Figure 4. TRMM 3B42v7 precipitation observations processed to show (a) mean annual precipitation (m yr^{-1}), (b) mean precipitation intensity (mm d^{-1}), (c) mean event duration (h), and (d) mean interval (days). Note the change in scale for mean annual precipitation and mean interval. Each grid cell is 0.25° × 0.25° (~27 km). Only grid cells with an average elevation of >600 m and that were less than 40% glaciated at the LGM are shown. Regions described in the main text are indicated as WF, western flanks; AL, Altiplano; and EF, eastern flanks. Altiplano lakes (Titicaca and Poopó) are outlined in black for spatial reference.

precipitation rates over mountainous regions were not adequately captured. Our analysis is based on TRMM observations from 2000 to 2011; years 1998 and 1999 were excluded because they have lower spatial coverage in each 3 h window. The TRMM data set is discretized with 3 h time steps, which we assume are representative of the 3 h window.

We calculate precipitation event metrics (Figure 3) that are commonly used in landscape evolution models from the precipitation time series. At each grid cell, consecutive time steps (3 h) with nonzero precipitation rates are grouped into precipitation events. Each precipitation event is then characterized by the mean precipitation rate (intensity, P) of the event, the duration (D) of the event, and the time interval (I) before the next event (Figure 3). The mean of each metric over all precipitation events is then calculated at each grid cell ($\overline{P}$, $\overline{D}$, and $\overline{I}$; Figure 4). Rainfall at a point can be described by a Poisson rectangular pulse model in which the duration, intensity, and time interval between events are all independent and exponentially distributed [*Eagleson*, 1978]. The probability distribution functions of these variables can then be fully described by the mean of that variable [*Eagleson*, 1978; *Tucker and Bras*, 2000]. The calculation of the mean over the entire record does not explicitly account for clustering of precipitation events in time, so the mean interval duration therefore also reflects seasonality.

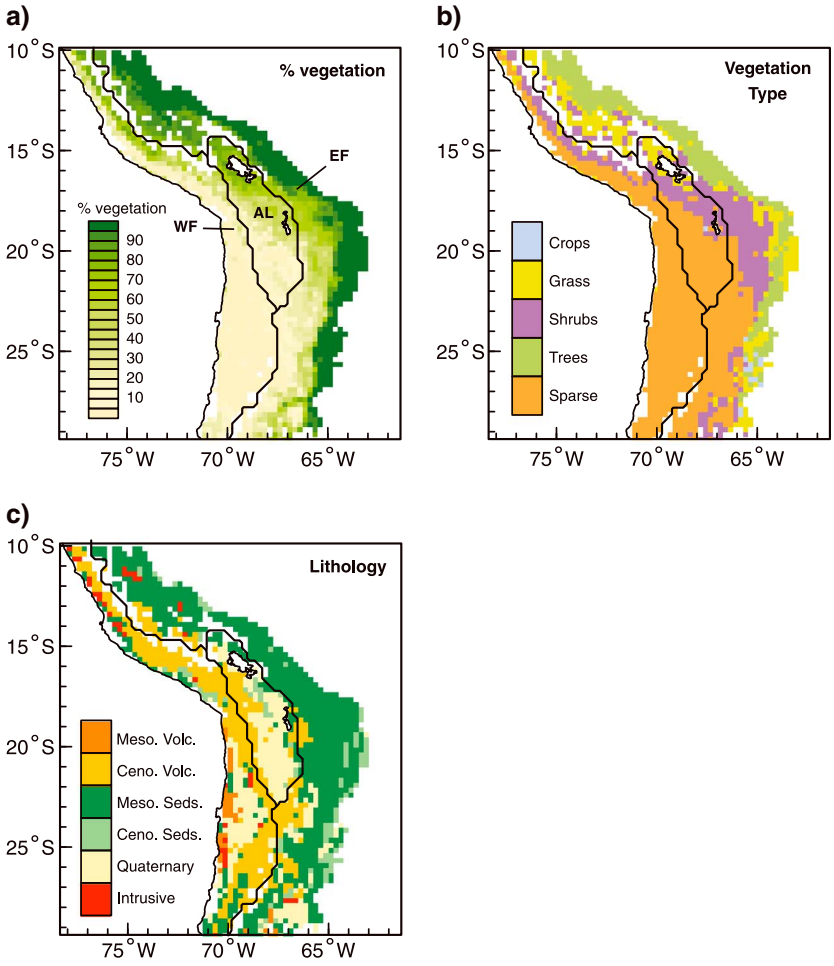

Figure 5. Land surface characteristics of the central Andes. (a) Percent vegetation cover and (b) modal vegetation type averaged from 0.05° resolution MODIS plant function type data set [*Lawrence and Chase*, 2007]. (c) Dominant bedrock lithology from USGS geologic maps [*Schenk et al.*, 1999]. Only grid cells with an average elevation of >600 m and that were less than 40% glaciated at the LGM are shown. Regions described in the main text are indicated as WF, western flanks; AL, Altiplano; and EF, eastern flanks. Altiplano lakes (Titicaca and Poopó) are outlined in black for spatial reference.

In addition, MAP is calculated directly from the TRMM observations. We can also assess how the intensity, duration, and interval components contribute to total MAP, as MAP can be approximated from the mean of the individual metrics according to

$$MAP = \overline{P} * \frac{\overline{D}}{\overline{D} + \overline{I}} * T_a. \quad (1)$$

where T_a is 1 year in units corresponding to $\overline{P}$ (modified after *Tucker and Bras* [2000]). Differences between directly calculated MAP and MAP derived from the individual statistics are small ($r^2 = 0.98$) and likely result from rounding errors in the calculations.

2.3. Vegetation Coverage

We use the vegetation data set developed by *Lawrence and Chase* [2007] from the Moderate Resolution Imaging Spectroradiometer (MODIS) instrument on NASA's Terra and Aqua satellites. In this derived data set, vegetation is classified into 17 Plant Functional Types (PFTs) at a grid spacing of 0.05°. The data set describes the percentage of each PFT including bare ground in each grid cell. We regrid this data set to the precipitation grid and reclassify the original PFTs to the following simpler subsets: "not vegetated," "shrubs," "grass," "trees," and "crops." This grouping simplifies the analysis yet maintains distinctions among major vegetation types. The "crops" class is not further discussed because the hillslope gradients at these locations are likely to reflect the

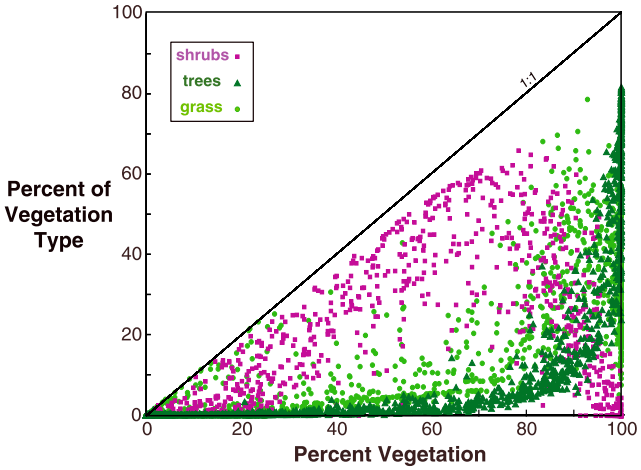

Figure 6. The type of vegetation varies with increasing vegetation cover. Shrubs are the dominant vegetation type where total vegetation is less than ~80%, with some grass mixed in. The fraction of grass cover increases with increasing vegetation and is most abundant between ~80 and 95% vegetation cover. Finally, trees dominate only in the most densely vegetated regions. Note that there are multiple data points at the same percent vegetation which may have different compositions in terms of type.

selection of land appropriate for crop growth. In the analysis, we present the total percent vegetation cover (Figure 5a) and the modal vegetation type in each grid cell (Figure 5b). If total vegetation cover is greater than 40%, the grid cell vegetation type is classified by the most abundant vegetation type (excluding "not vegetated").We include "not vegetated" as an option for the modal vegetation type when the grid cell is <40% vegetated. We do not include this option for >40% vegetated because the vegetation in some cells is composed of multiple vegetation types that individually have a lower cover than the bare ground but in combination can reach >70% total vegetation cover. A cutoff anywhere between 30 and 50% may be chosen, and the choice would mostly affect statistics for the shrubs category because this is the dominant vegetation type in the more sparsely vegetated regions (Figure 6). We later show that percent vegetation is a more useful variable than vegetation type, so the choice of cutoff does not significantly affect the results.

2.4. Surface Geology

Lithological data from the USGS [*Schenk et al.*, 1999] are also reclassified and regridded (Figure 5c) to match the TRMM resolution. We distinguish between lithological types based on their physical strength. To do so, we first separate them according to general rock type (sedimentary, volcanic, intrusive, and metamorphic) and then by age (Quaternary, Cenozoic, and Mesozoic). We recognize that these divisions do not account for all lithological variations (e.g., differences between shales and sandstones) or for structural variations (e.g., differences in the extent of rock fracturing) [*Duhnforth et al.*, 2010; *Larsen et al.*, 2010]. However, at the resolution of the precipitation data, these categories serve as a useful starting point for differentiating among different rock strengths.

2.5. Data Set Analysis Methods

Grid points that have been affected by recent glaciations or have not experienced recent tectonic activity are excluded from our analysis. Grid cells in which >60% of the area was covered by glaciers at the Last Glacial Maximum [*Ehlers et al.*, 2011] or with a mean elevation less than 600 m are removed to restrict the analysis to the nonglaciated, active mountain belt. After removal of these data, 1739 grid points remain.

The strength of correlations among topography, vegetation, and climate variables is explored quantitatively using Pearson's correlation coefficient and visualized using scatterplots. Correlation coefficients are used to identify linear correlations and to compare the strengths of linear relationships between different variable pairs and subsets. Unless otherwise stated, all correlation coefficients are reported at the $p < 0.01$ significance level according to a two-tailed test. Correlation coefficients alone are only able to identify linear relationships; scatterplots allow the identification of nonlinear trends and outliers. The analysis is presented in the following order: (1) observational data; (2) direct correlations between hillslope gradients and precipitation metrics, vegetation, and lithology; and (3) exploration of interdependence between climate and vegetation controls on hillslope gradients using data subsets and multiple linear regression models.

3. Results

3.1. Observed Precipitation, Topography, Vegetation, and Geology Characteristics

3.1.1. Topography

Highest mean hillslope gradients (>24°) are found in the northern Central Andes, particularly the northeastern flanks (north of ~17°S, Figure 2). Peak mean hillslope gradients are associated with large,

deeply incised drainage networks such as the upper catchment of the Río Beni on the northeastern flanks. Canyons are also the primary location of high hillslope gradients on the western flanks, e.g., the Cotahuasi-Ocoña canyon at ~16°S. Peak hillslope gradients in the southeastern flanks are also associated with river valleys (Río Pilcomayo and Río Grande), but maximum values are lower (~20–24°). The Altiplano has consistently low mean hillslope gradients (<10°), as does the Atacama region of the western flanks (20–27°S).

3.1.2. Precipitation

Mean annual precipitation derived from the TRMM 3B42v7 data set (Figure 4) is consistent with the magnitudes and spatial distributions of MAP in other observational data sets [*Bookhagen and Strecker*, 2008; *Houston and Hartley*, 2003; CRU, *Hulme*, 1992]. MAP rates are highest on the northeastern flanks (north of 18°S, Figure 4a) and decrease with increasing elevation from ~3–5 m yr^{-1} at ~600 m elevation to less than 2 m yr^{-1} near the drainage divide. Further south (>18°S) on the eastern flanks, MAP is less than 2 m yr^{-1} and the relationship with elevation is weaker. MAP on the eastern Andean flanks is high because (1) Andean topography deflects moisture transport southward from the Amazon basin, driving the South American Low Level Jet, and (2) orographic lifting induces convective precipitation [*Campetella and Vera*, 2002; *Insel et al*., 2010a]. In contrast, MAP on the western flanks is extremely low (<1 m yr^{-1}) at all latitudes with much of the region receiving less than 0.1 m yr^{-1}. Hyperarid conditions on the western flanks are attributed to (1) the subtropical location in the descending branch of the Hadley cell [*Rutllant et al*., 2003], (2) blocking of moisture by the Andes, and (3) the presence of the cold, Humboldt Current that generates a temperature inversion at the coast and traps moisture below ~800 m [*Houston and Hartley*, 2003].

Over the study area, MAP calculated directly and MAP estimated from event metrics (equation (1)) agree strongly ($r^2 = 0.98$) within the study area. MAP is a combination of *P*, *D*, and *I* components, but the relative importance of each component varies spatially across the Andes (Figure 4). Similarly to MAP, precipitation intensity increases from west to east, with peak intensities (>45 mm d^{-1}) occurring on the eastern flank at 13°S. However, precipitation intensity does not have the same north-south variability as MAP on the eastern flanks. Instead, precipitation intensity decreases from >30 mm d^{-1} at the lowest elevations to <15 mm d^{-1} at the drainage divide along the length of the orogen. Precipitation events north of 18°S on the eastern flanks have a longer average duration and occur more frequently (Figures 4c and 4d), and in this location, MAP is more dependent on these variables (equation (1)). A similar north-south pattern is observed on the arid western flanks.

3.1.3. Vegetation

Total vegetation cover increases strongly from west to east (Figure 5a) and on the western flanks also displays a weaker south to north gradient. Vegetation patterns strongly reflect regional climate, with higher vegetation cover corresponding to higher MAP (Figures 4a and 5a). The transition from low to high percent vegetation cover is typically accompanied by a progression from bare ground to shrubs, grasses, and finally trees (Figures 5b and 6). Shrubs border desert regions, and also cover a large area of the northern Altiplano and high elevations on the eastern flanks between 17 and 22°S. Between ~80% and 95% vegetation cover, the abundance of shrubs declines and the proportion of grassland in each grid cell reaches a broad peak. Over the same range, the abundance of trees also increases, and above ~95% total vegetation cover, trees are the dominant vegetation type. Grasses are the most abundant vegetation type at high (> ~ 2 km) elevations north of 17°S at (Figures 5 and 6). The lower elevations are covered by a mixture of grass and trees south of 17°S, but north of 17°S, trees dominate the vegetation cover (Figures 5a and 5b). These spatial patterns are revisited in more detail in the correlation and regression analyses presented later (sections 3.2 and 3.3).

3.1.4. Bedrock Lithology

Bedrock lithology of the central Andes varies significantly between the different geographic regions (Figure 5c). The eastern flanks are dominantly underlain by Paleozoic to Mesozoic sediments. The youngest sediments are currently being uplifted at the eastern margin of the fold-and-thrust belt. Cenozoic volcanic deposits of the western Cordillera dominate higher elevations in the western flanks. Large Quaternary sedimentary basins include the Altiplano and Atacama. Additional Quaternary sediments are found in fault-bounded basins on the eastern flanks (south of ~22°S). The "Quaternary" group also encompasses Quaternary volcanoes and volcanic deposits, most of which are not large enough to dominate a grid cell. Minor intrusive and older volcanic rocks can be found on the Pacific Coast and scattered elsewhere.

Table 1. Correlation Coefficients Between Mean Hillslope Gradient and Precipitation Metrics[a]

	Pearson's Correlation Coefficient					
Classification	Mean Annual Precipitation (m yr^{-1})	Mean Event Intensity (mm d^{-1})	Mean Event Duration (h)	Mean Interval Duration (days)	Vegetation Cover (%)	Number of Data Points
All data	0.49	0.26	0.52	−0.32	0.56	1739
WF and EF	0.52	0.22	0.49	−0.44	0.58	1465
			Region			
Eastern Flank	0.48	-	0.45	−0.59	0.50	934
Altiplano	-	*-0.14*[b]	0.44	−0.37	0.23	269
Western Flank	0.45	0.34	0.28	−0.35	0.60	531
			Percent Vegetation (WF and EF Only)			
0–95%	0.60	0.31	0.55	−0.42	0.69	1116
95–100%	0.34	−0.56	0.32	−0.69	−0.31	349
			Modal Vegetation Type (WF and EF Only)			
Not vegetated	0.19	-	0.16	−0.24	0.38	692
Shrubs	0.32	-	0.25	−0.36	0.42	287
Grass	0.46	−0.49	-	−0.67	-	204
Trees	0.16	−0.54	-	−0.55	0.36	269
Crops	-	−0.82	−0.88	-	-[c]	13
			Lithology (WF and EF Only) [d]			
Quaternary	0.35	-	0.23	−0.23	0.47	183
Cenozoic Sed.	*0.26*[b]	*−0.24*[b]	-	−0.46	-	93
Older Sed.	0.45	0.10	0.44	−0.40	0.51	738
Cenozoic Volc.	0.34	0.13	0.29	−0.29	0.57	372
Mesozoic Volc.	-	0.48	-	-	0.72	39
Intrusive	0.59	*0.37*[b]	0.51	−0.54	0.52	40

[a]Pearson's correlation coefficients are given for all data and data separated according to percent vegetation, modal vegetation type, and modal lithology. All correlations are statistically significant at the $p < 0.01$ level according to a two-tailed test, unless otherwise indicated. Correlations that are not significant at the $p<0.01$ level but are significant at the $p<0.05$ level are shown in Italics, and for correlations coefficients that are not significant at the $p < 0.05$ level, no values are reported.
[b]Correlation is significant at the $p < 0.05$ level according to a two-tailed test but not at $p < 0.01$.
[c]Cropland expected to change natural percent vegetation cover.
[d]Abbreviations for lithologies are as follows: Sed., sedimentary rocks; Volc., volcanic rocks; "Older," older than Cenozoic.

3.2. Correlation Analysis

3.2.1. Correlations Between Precipitation Metrics and Hillslope Gradients

Statistical analysis of precipitation metrics shows that mean hillslope gradients in the central Andes are most strongly correlated with mean event duration ($r = 0.52$, Table 1) and mean annual precipitation ($r = 0.49$). Correlations between mean hillslope gradient and mean event intensity and mean interval duration are lower ($r = 0.26$ and $r = -0.32$, respectively). However, it is evident from scatterplots (Figure 7) that relationships between mean hillslope gradient and precipitation are not linear. We begin a more rigorous interrogation of the data set by subsetting the observations according to geographic regions (western and eastern flanks, and the Altiplano; section 2.1 and Figure 2a) that are characterized by different climatic regimes and dominant bedrock lithology.

Mean hillslope gradient generally increases with mean annual precipitation (Figure 7a). As MAP increases, the upper bound of observed hillslope gradients increases from <20° at <0.1 m yr^{-1} MAP to ~32° at 2 m yr^{-1} MAP. Over the same range in MAP, the lower bound of observed hillslope gradient changes little. However, where MAP exceeds 2 m yr^{-1}, mean hillslope gradients are everywhere greater than ~10°. High (>25°) hillslope gradients are found on both flanks (Figure 7) but not on the Altiplano (<13°). This difference likely reflects the presence of erosional processes on the flanks and depositional processes on the Altiplano. Correlation coefficients between hillslope gradient and MAP are stronger on individual flanks ($r >$ =0.45, Figure 7a and Table 1) than on the Altiplano ($r = 0.12$). The best fit linear relationship between mean hillslope gradient and MAP is marginally greater on the eastern flank than the western flank ($r^2_{west} = 0.2$ and $r^2_{east} = 0.23$, respectively).

Precipitation intensity ($\bar{P}$) and mean hillslope gradient are not strongly correlated over the entire domain ($r = 0.26$, Table 1) or across geographic regions ($|r| <$ = 0.34, Figure 7b). In part, this is because mean hillslope

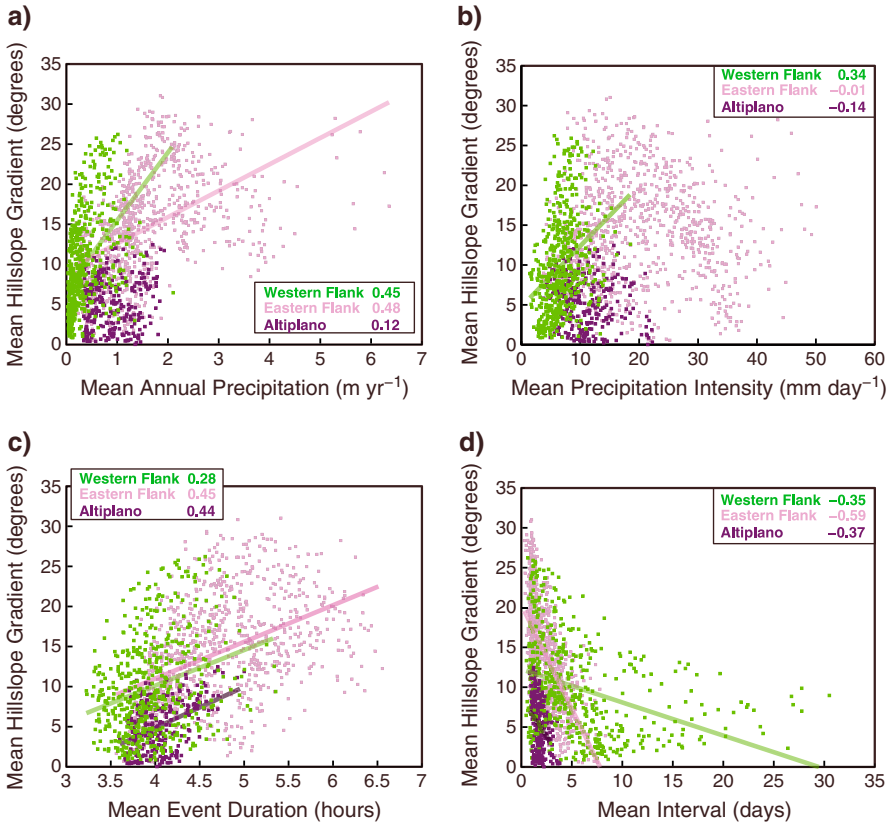

Figure 7. Scatterplots of mean hillslope gradient (Figure 2b) against TRMM derived precipitation metrics (Figure 4). (a) Mean annual precipitation (m yr^{-1}), (b) mean precipitation intensity (mm d^{-1}), (c) mean event duration (h), and (d) mean interval duration (days). Observations are subdivided according to geographic region (Figure 2a): western flank (green), eastern flank (light purple), and Altiplano (dark purple). Correlation coefficient (r) between mean hillslope and precipitation metric is given for each region, and best fit lines are shown for subsets in which $|r|$ exceeds 0.25.

gradient and precipitation intensity do not have a simple linear relationship (Figure 7b); mean hillslope gradient increases at precipitation intensities < 20 mm d^{-1} but decreases at higher intensities. Over the entire observational data set, mean hillslope gradient is most strongly linearly correlated with mean event duration ($r = 0.52$, Table 1). Correlation coefficients are lower for individual geographic regions than for the whole data set, but the best fit linear relationship has a similar slope (4.7°/h) for all three regions (Figure 7c). Finally, mean hillslope gradients generally decrease with increasing mean event interval ($\bar{I}$, Figure 4d and Table 1). Mean interval ($\bar{I}$) is not strongly correlated with hillslope gradients for the complete data set ($r = -0.32$) or on the Altiplano or western flank ($r = -0.37$ and $r = -0.35$, respectively, Figure 7d). However, the correlation coefficient between $\bar{I}$ and hillslope gradients on the Eastern Flank is -0.59, the highest correlation found in our regional analysis.

No single precipitation metric can explain the spatial variation in mean hillslope gradient. In general, mean hillslope gradients increase with increasing MAP and event duration and decrease with mean interval. Some precipitation metrics have a stronger correlation with hillslope gradient when individual regions are considered, e.g., mean interval on the eastern flanks ($r = -0.59$, Table 1). These initial findings contradict modeling and observational studies that precipitation intensity is a strong control on landscape morphology [*Tucker*, 2004; *Tucker and Bras*, 2000]. Because hillslope gradients on the Altiplano are low, and because depositional processes are more important than uplift and erosion in this region, we focus on the western and eastern flanks for the remainder of the study.

3.2.2. Hillslope Dependence on Vegetation

Mean hillslope gradients are more strongly correlated with vegetation cover than any of the precipitation metrics over the whole domain ($r = 0.56$, Table 1). The range of mean hillslope gradients increases with the

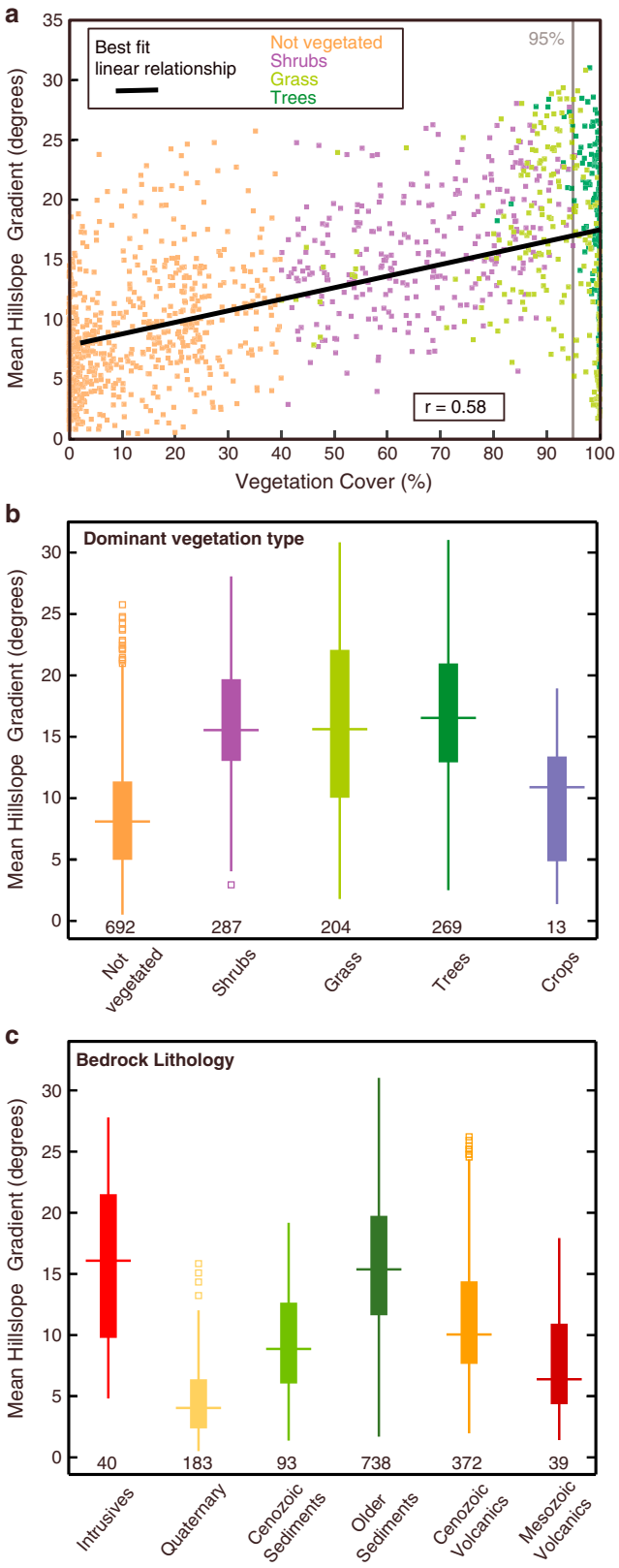

Figure 8

percent of vegetation cover from 0 to 20° where there is no vegetation cover to hillslope gradients of 0–32° at 100% vegetation cover (Figure 8a). The relationship between hillslope gradient and vegetation cover appears linear; mean hillslope gradients increase with vegetation cover to ~80%, but as vegetation cover increases further, the relationship deteriorates and lower hillslope gradients (<10°) are common.

As vegetation cover increases, the modal vegetation type transitions from bare ground to shrubs, grasses, and finally trees at > ~95% vegetation cover (Figure 7a). Below ~80% vegetation cover, an increase in vegetation cover primarily reflects an increase in shrubs, with some increase in grass cover (Figure 6). Shrub coverage decreases steeply to <5% between 80 and 100% total vegetation cover. Trees are almost absent where total vegetation cover is less than 80%; tree cover increases rapidly above 80% to become the dominant functional type at 100% vegetation. Classifying vegetation cover by plant functional type does not directly help to predict mean hillslope gradient (Figure 8b). Where surface cover is classified as not vegetated, mean hillslope gradients are low (mean of ~13°), but the distribution of mean hillslope gradient is similar for shrubs, grass, and trees (Figure 8b). The lower hillslope gradients associated with agricultural land ("crops," Figure 8b) are interpreted as a cause, not a consequence, of the land cover type. Although different vegetation types are expected to affect the landscape via different mechanisms, a clear relationship between vegetation type and mean hillslope gradient is not apparent in the central Andes. For example, similar means and ranges of hillslope gradients are found for shrubs, grass, and trees (Figure 8b).

3.2.3. Hillslope Dependence on Bedrock Lithology

In contrast, mean hillslope gradients show a strong association with bedrock lithology (Figure 8c). Mean hillslope

Table 2. Correlation Coefficients Between Percent Vegetation Cove and Precipitation Metrics[a]

	Pearson's Correlation Coefficient				
Classification	Mean Annual Precipitation (m yr^{-1})	Mean Event Intensity (mm d^{-1})	Mean Event Duration (h)	Mean Interval Duration (days)	Number of Data Points
All data	0.77	0.74	0.81	−0.43	1739
EF and WF	0.77	0.75	0.82	−0.47	1465
		Percent Vegetation (WF and EF Only)			
0–95%	0.79	0.56	0.75	−0.48	1116
95–100%	*0.11*[b]	0.39	0.27	-	349
		Modal Vegetation Type			
Not vegetated	0.59	0.45	0.27	−0.33	692
Shrubs	0.48	0.36	0.59	−0.18	287
Grass	0.28	0.60	0.63	-	204
Trees	-	0.35	0.29	*0.15*[b]	269

[a]Pearson's correlation coefficients are given for all data and data separated according to percent vegetation and modal vegetation type. All correlations are statistically significant at the $p < 0.01$ level; according to a two-tailed test, unless otherwise indicated. Correlations that are not significant at the $p<0.01$ level but are significant at the $p<0.05$ level are shown in Italics, and for correlations coefficients that are not significant at the $p < 0.05$ level, no values are reported.
[b]Correlation coefficient is significant at the $p < 0.05$ level according to a two-tailed test but not at $p < 0.01$.

gradients are highest where underlain by intrusive rocks or Mesozoic and Paleozoic sedimentary rocks. Lower hillslope gradients are generally found on younger sedimentary rocks and Quaternary sediments. Low hillslope gradients in Quaternary sediments are likely due to the depositional nature of the systems. The opposite is true for volcanic rocks in that higher hillslope gradients are found in regions underlain by the younger (Cenozoic) rocks, although there is significant overlap in the range of hillslope gradients found in these two broad age categories. Higher hillslope gradients are generally found on substrates that are less susceptible to erosion [*Aalto et al*., 2006].

3.3. Interdependent Controls on mean Hillslope Gradients

Percent vegetation cover and lithology exert the strongest influence on mean hillslope gradient in the central Andes. However, a high degree of scatter exists in the data that cannot be explained by these two factors alone. Below we consider the interaction of different climate and vegetation properties by subsetting the data.

3.3.1. Vegetation Categories

Although vegetation shows the strongest correlation with mean hillslope gradient, vegetation is dependent on climate (Table 2). The high correlation between MAP and percent vegetation cover ($r = 0.77$, Table 2) is consistent with moisture availability being the limiting factor on net primary productivity in the Central Andes [*Churkina and Running*, 1998]. Other factors, including surface temperature, nutrient availability, and solar radiation, may explain the remaining spatial variability in vegetation cover [*Churkina and Running*, 1998]. Maximum correlation coefficients between both vegetation and climate variables and hillslope gradients are found when observations are categorized into groups with vegetation cover above and below 95%. Where vegetation cover is less than 95%, mean hillslope gradient is highly correlated with MAP ($r = 0.60$, Table 1 and Figure 9), but mean hillslope gradient also correlates with percent vegetation cover ($r = 0.69$, Table 1). For this same vegetation category (i.e., <95% cover), vegetation and MAP are also strongly correlated ($r = 0.79$, Table 2). The correlation coefficients suggest that for this subset of the data, the relationship between precipitation and vegetation, and hillslope gradients is strongly coupled.

Figure 8. (a) Mean hillslope gradient (degrees, Figure 2b) against percent vegetation cover (Figure 5a) color-coded according to modal vegetation type. Black line indicates the best fit linear relationship. However, this relationship breaks down at >95% vegetation where lower slopes are again found. (b) Boxplots of mean hillslope gradient, subdivided by modal vegetation type (Figure 5b). Number of data points in each group is indicated at the base. (c) Boxplots of mean hillslope gradient, subdivided by modal bedrock lithology (Figure 5c). Number of data points in each group is indicated at the base. Observations in these plots are from the western and eastern flanks only.

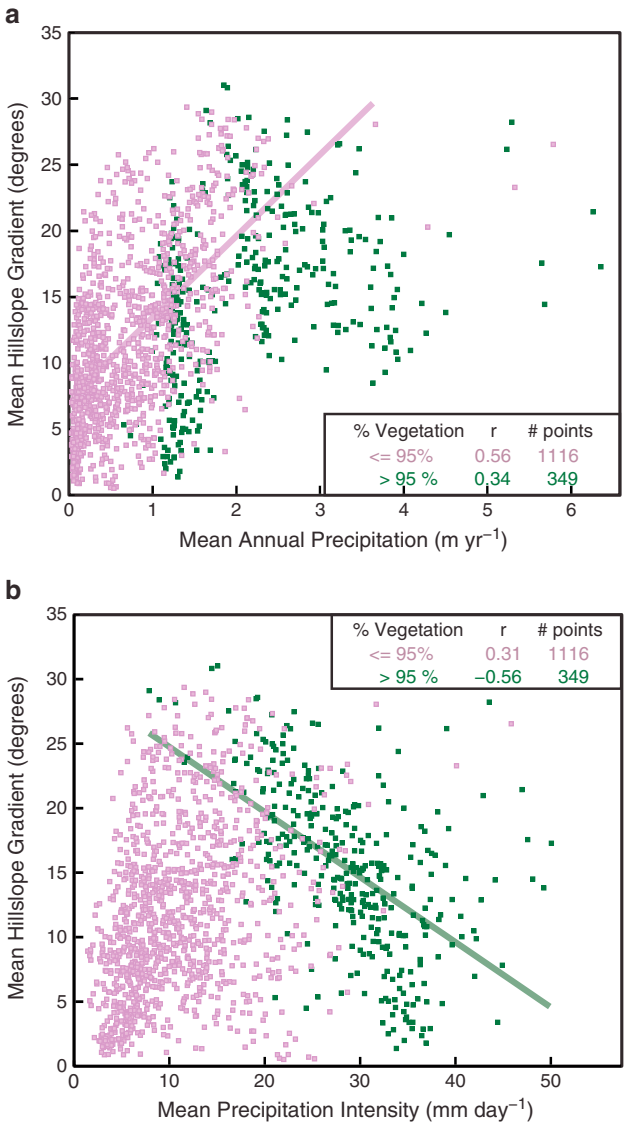

Figure 9. Scatterplots of mean hillslope gradient versus precipitation metrics (first shown in Figure 7) color coded according to amount of vegetation cover. (a) Mean annual precipitation correlates more strongly with hillslope gradient where vegetation cover is less than 95% (light purple). (b) Conversely, mean precipitation intensity correlates more strongly with hillslope gradients where vegetation cover exceeds 95 % (dark green). Observations in these plots are from the western and eastern flanks only.

In contrast, when >95% of the landscape is covered by vegetation, both MAP and percent vegetation are poorly correlated with mean hillslope gradients ($r_{MAP} = 0.34$ and $r_{veg} = -0.31$, Table 1). At vegetation cover above 95%, we observe an expansion of the range of hillslope gradients (2–32°, Figures 8a and 9), suggesting that other factors determine hillslope gradients in these regions. Correlation analyses show that mean hillslope gradient correlates most strongly with mean precipitation intensity $(\overline{P})$ and interval between events $(\overline{I})$ under dense vegetation cover ($r_P = -0.56$ and $r_I = -0.69$, Figure 9b and Table 1). In summary, where vegetation density is high and no longer responds to increasing moisture availability, the effects of changing precipitation on hillslope gradients are not modulated by vegetation and precipitation intensity and interval are the important precipitation variables.

3.3.2. Multiple Linear Regression Analysis

Our correlation analyses indicate that multiple variables correlate with hillslope gradients in the central Andes. Stepwise multiple linear regression analyses are performed to determine whether a combination of variables can better explain variability in observed hillslope gradients than a single variable. Models were evaluated based on r^2 and F-statistic values. The F-statistic evaluates whether the model is better than the null hypothesis that the coefficient of all variables is zero. Acceptable models all have individual variable coefficients that are both significant at the 1% level and are reasonable with respect to the original correlation analyses. Models with more variables or with variable transformations, e.g., logarithmic or exponential, are not presented because they did not explain any additional variability in the observations. Lithology was not included as a variable in the regression modeling because the lithological data are qualitative, not quantitative.

In the <95% vegetation category, the best fit regression model incorporates percent vegetation cover and precipitation intensity and has an r^2 of 0.49 (Figure 10a):

$$Hillslope\ Gradient_{<95\%} = 7.96 - 0.12 * \overline{P} + 0.15 * \%veg \quad (2)$$

This model represents only a marginal improvement over the linear regression between vegetation cover and hillslope ($r^2 = 0.48$). The precipitation intensity coefficient is negative in (2) indicating that precipitation

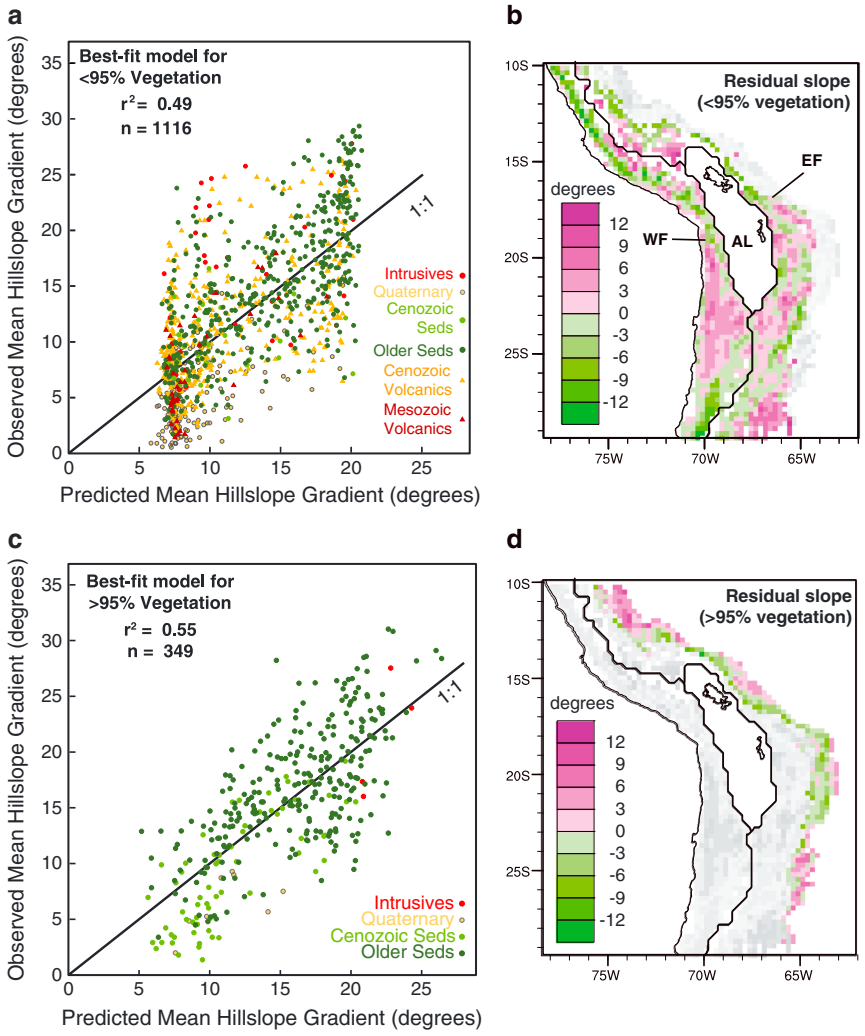

Figure 10. Comparison of observed and predicted hillslope gradients for the best multiple linear regression models found for (a and b) <95% vegetation category and (c and d) >95% vegetation category. A 1:1 ratio (black line) is shown to aid comparison (Figures 10a and 10c); points above the line indicate hillslope gradients that are underestimated by the multiple linear regression model. Each data point is color coded according to bedrock lithology at that point. Maps of the spatial distribution of the residual hillslope gradients (Figures 10b and 10d), that is the predicted slope minus the observed slope, indicate where the regression model overestimates (magenta) and underestimates (green) observed mean hillslope gradients (see Figure 2b). The regression model is only applied to the appropriate geographic locations; data points belonging to the other vegetation subset are shown in grey.

intensity works in opposition to vegetation cover. Some of the additional variability in mean hillslope gradient that is not captured in the model may be explained by spatial variations in bedrock lithology (Figure 10a). The model does not do a good job at predicting low (<6°) hillslope gradients, in part because a large number of data points have very low vegetation cover and the predictive capabilities of the model saturate where vegetation is approximately constant. Hillslope gradients that are overestimated by the regression model are also commonly on Quaternary or Cenozoic sediments, which are likely to be weaker and more easily eroded (Figures 10a and 10b). For example, the model overpredicts hillslope gradients in the Atacama basin and on the eastern flanks south of 27°S (Figures 5c and 10b). In contrast, the model underpredicts hillslope gradients on the northwestern flanks (1–16°S) where deeply incised canyons dominate the topography. In this region, precipitation rates decrease strongly downstream and much of the discharge derives from the headwaters [*Jeffery et al.*, 2013]. Closer to the coast, channel incision rates depend on the integrated effects of the entire upstream drainage area, whereas hillslope erosion is more dependent

on the local, arid, precipitation conditions. We suggest that this region reflects a transient case (Figure 1e) in which high hillslope gradients result from oversteepening of hillslopes close to the rapidly incising channel.

The best fit model for the >95% vegetation category includes mean precipitation intensity and mean interval and has an r^2 of 0.55 (Figure 10c):

$$Hillslope\ Gradient_{>95\%} = 29.8 - 0.28 * \overline{P} - 2.89 * \overline{I} \quad (3)$$

As in the sparse vegetation category, hillslope gradients are overestimated on Quaternary and Cenozoic sediments (Figure 10c). Again, $\overline{P}$ is negative, but $\overline{I}$ is also negative suggesting that less frequent events have a greater erosional efficiency. In the seasonal climate on the eastern flanks of the central Andes, high interval duration may be indicative of the highly seasonal rainfall rather than simply infrequent events. The >95% regression model tends to overpredict hillslope gradients at lower elevations and particularly between 10–12°S and 24–26°S (Figure 10d). As with the <95% regression model, a coherent spatial pattern exists in the residual between predicted and observed hillslope gradients. This spatial clustering may be due to the influence of bedrock lithology (Figure 5c), such as an overestimation of hillslope gradients in sedimentary basins and where younger sediments have not yet been eroded. In the following discussion, we explore the physical mechanisms underlying the relationships among vegetation, climate, and hillslope gradients in these two vegetation categories.

4. Discussion

In the central Andes, mean hillslope gradients correlate more strongly with vegetation cover ($r = 0.56$, all data, Table 1) than any individual precipitation metric. However, vegetation cover also correlates strongly with precipitation (Table 2), suggesting more complex interactions between these three variables. The strongest relationships between topography and precipitation emerge when the data set is divided into two categories, partially (<95%) and fully (>95%) vegetated (Figure 8). Within these categories, some variation in mean hillslope gradient can be explained by the underlying bedrock lithology (Figure 5c). In the following sections, we explore (1) possible physical mechanisms underlying the observations, (2) additional factors that affect hillslope gradients that might explain scatter in the observed relationships, and (3) how these observations can inform future research avenues.

4.1. Climatic Erosional Efficiency, Erosion Resistance, Rock Uplift, and Equilibrium Landscapes

In an equilibrium landscape, mean hillslope gradients adjust such that catchment wide erosion rates balance rock uplift. Any decrease in climatic erosional efficiency, or increase in erosional resistance, requires higher hillslope gradients to attain the same catchment scale erosion rates (Figure 1). In transient landscapes, channels may respond to a change in base level faster than hillslopes, and as a result high interfluve relief will develop (Figure 1e). High hillslope gradients can therefore indicate low climatic erosional efficiency, high erosional resistance, high uplift rates, and/or high channel incision rates relative to hillslope erosion rates. A major challenge in the study of climate-tectonics-landscape interactions is in identifying which of these factors is the most important and under what conditions. A number of studies [*Carretier et al.*, 2013; *Aalto et al.*, 2006] find high correlations between catchment-scale erosion rates and hillslope gradients, suggesting that catchment morphology is primarily responding to spatial variations in uplift rate until threshold hillslopes are attained [*DiBiase et al.*, 2012; *Larsen and Montgomery*, 2012]. Catchment erosion rates have been found to both correlate with mean annual precipitation [*Bookhagen and Strecker*, 2012; *Owen et al.*, 2010] and to not correlate with local climatic variables [*Aalto et al.*, 2006; *Insel et al.*, 2010b; *Riebe et al.*, 2001]. In this study, we find significant correlations between rainfall, vegetation, and geomorphic properties at the orogen scale. The influence of climate and vegetation on mean hillslope gradients in the central Andes may be better understood by considering the physical mechanisms underlying the observed statistical relationships. The statistical relationships between the variables considered differ between partly and fully vegetated landscapes, so these categories are considered separately below.

4.1.1. Low-Density Vegetation: MAP, Vegetation, and Hillslope Gradients

Where vegetation is less than 95%, an increase in MAP is accompanied by an increase in vegetation cover ($r = 0.79$, Table 2). As MAP and vegetation increase, mean hillslope gradients also increase. These statistical relationships may be interpreted in a number of ways, including (1) MAP and vegetation are determined by the regional climate and modify hillslope stability and thereby hillslope gradients and (2) tectonic processes

build high relief which promotes high precipitation and consequently vegetation density. In more detail, increasing MAP and vegetation cover has three potential effects on hillslope gradients: (1) Increasing MAP increases moisture available for surface runoff. Enhanced runoff is expected to increase erosion potential and result in lower hillslope gradients in an equilibrium landscape (Figure 1c). (2) An increase in vegetation will reduce surface runoff by increasing infiltration rates and by intercepting rainfall before it hits the ground. (3) Greater rooting increases cohesion of the subsurface and increases surface roughness, thereby increasing erosional resistance [*Wainwright et al*., 2000]. These two effects of vegetation are to both decrease climatic erosional efficiency and increase resistance of the hillslopes, requiring higher hillslope gradients in an equilibrium landscape. Our observations indicate that mean hillslope gradients generally increase with an increase in MAP that is accompanied by increasing vegetation cover. According to the expected impacts of increasing MAP and vegetation on hillslope gradients at equilibrium, these observations suggest that the physical effects of vegetation cover outweigh those of increasing MAP and that in the $<$95% vegetation category, the primary control of climate on topography is through changing vegetation cover, for a particular erosion rate. This interpretation is consistent with catchment-scale modeling studies that suggest hillslope gradient responses to climate are moderated by vegetation [*Collins and Bras*, 2010].

An alternative interpretation of the correlation between MAP, vegetation cover, and hillslope gradients is that high uplift rates result in high relief which drives increases in precipitation [e.g., *Bookhagen and Strecker*, 2008] and consequently increased vegetation cover. In this interpretation, the correlation between MAP, vegetation cover, and hillslope gradients is a result of the effects of topography on atmospheric circulation rather than the impacts of climate on the landscape. If erosion rates are taken as a proxy for uplift rates (assuming topographic equilibrium), then a strong correlation between hillslope gradients and erosion rates would support the latter hypothesis. Across different timescales of measurement and location, existing erosion rate data sets in the central Andes have either a positive [e.g., *Carretier et al*., 2013; *Aalto et al*., 2006] or no [e.g., *Insel et al*., 2010b; *Safran et al*., 2005] correlation with hillslope gradients. Distinguishing between the two interpretations is therefore difficult with existing observations, and it is possible that both mechanisms are occurring. The fact that the relationships between vegetation, precipitation, and topography exist across both the western and eastern flanks, and therefore substantially different tectonic regimes, supports the first interpretation of vegetation modulating hillslope gradients at this scale. Further understanding may be gained by examining the timescale of responses. If the timescale of response of hillslope stabilization to vegetation change is faster than the hillslope response to changes in tectonic deformation, then vegetation is likely to be the dominant control.

4.1.2. Dense Vegetation: Elevation, Interval, Intensity, and Hillslope Gradients

Under full vegetation coverage, an increase in MAP does not result in a significant increase in vegetation density. As vegetation cover is at a maximum, additional indirect loss of moisture to infiltration or canopy interception, or increase in erosion resistance with changing precipitation is limited. Under dense vegetation cover, mean hillslope gradients correlate most strongly with interval duration ($r = -0.69$) and precipitation intensity ($r = -0.56$). In addition, mean hillslope gradients also correlate highly with mean elevation ($r = 0.74$) in this vegetation category despite elevation correlating poorly with hillslope gradients in all other categories explored (see supporting information). As with the partly vegetated category, multiple possible interpretations are consistent with the observations.

Elevation in itself is not a control on hillslope gradients; rather, it is likely to serve as a proxy for another variable that changes with elevation. On the densely vegetated eastern flanks, it may serve as an indicator of relief on the fluvial network. The high correlation observed could indicate that at high-elevation hillslopes have not equilibrated to the change in base level as quickly as the channels (Figure 1e). However, an increase in elevation also correlates with age of deformation, decreasing temperatures, decreasing precipitation intensity, and possibly vegetation changes not captured in the MODIS data set. One or a combination of the above variables could be the underlying cause of the correlation between elevation and hillslope gradients in this region.

In the dense vegetation category, mean hillslope gradient also correlates with mean interval duration ($r = -0.69$). Further insight may be gained by separating the data into regions north and south of 17.5°S (Figure 11). North of 17.5°S, the mean interval is less than 2 days, and hillslope gradients correlate poorly with $\bar{I}$ ($r = -0.23$) with a range in hillslope gradients of 8–32°. South of 17.5°S, hillslope gradients decrease from 15–25° at $\bar{I}$ = 2 days to 0–10° at $\bar{I}$ = 4.5 days ($r = -0.62$). A possible explanation of the correlation between

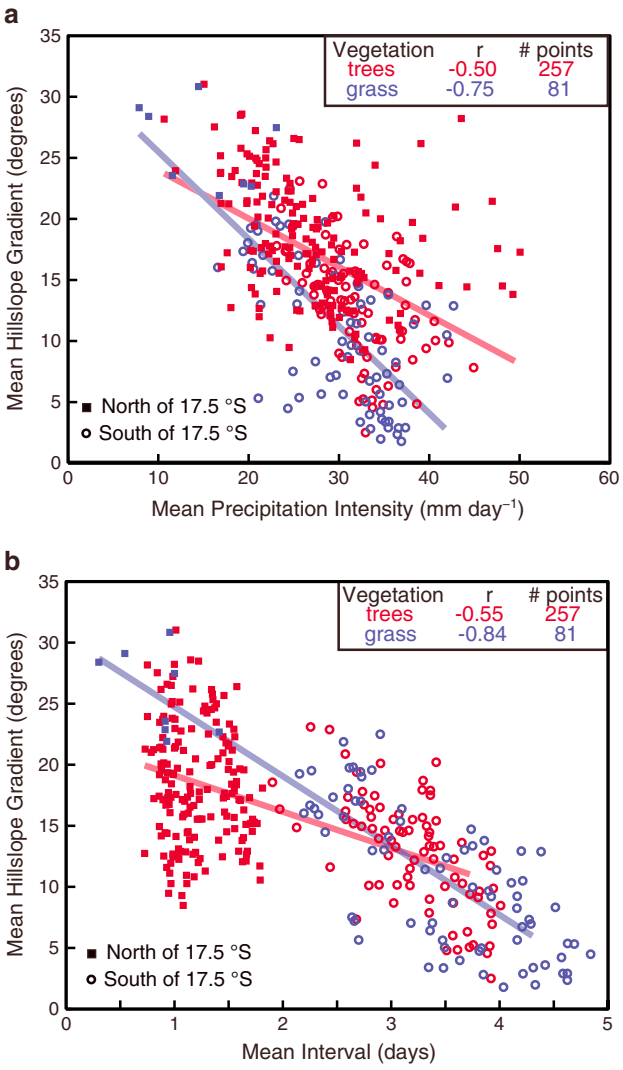

Figure 11. Scatterplots of hillslope gradients versus precipitation metrics in densely vegetated (>95%) regions, color coded according to most abundant vegetation type: trees (red) and grass (blue). (a) Mean hillslope gradient decreases with increasing precipitation intensity. (b) Mean hillslope gradient generally decreases with mean interval, but hillslope gradients span a broad range (8–32°) where precipitation events occur almost daily (north of 17.5°S, filled squares).

hillslope gradient and $\bar{I}$ is that temporal clustering of precipitation events plays a role in determining erosional efficiency. The occurrence of landslides in particular is dependent on antecedent conditions, in addition to individual precipitation events [*Crozier*, 1999; *Gabet et al.*, 2004]. The data presented here are consistent with a seasonal fluctuation between dry and wet conditions being more erosive than a year-round wet environment.

Finally, mean hillslope gradients decrease from ~25° at precipitation intensities of $\bar{P} = 10$ mm d^{-1} to ~10° at $\bar{P} = 40$ mm d^{-1} ($r = -0.56$, Figure 9b). As $\bar{P}$ increases, surface runoff and erosional efficiency increase, resulting in lower hillslope gradients. The modal vegetation type can explain some additional variability in the relationship between $\bar{P}$ and mean hillslope gradient (Figure 11a); trees are associated with slightly higher (4–5°) hillslope gradients than grass. A possible reason is that grass modifies the geomorphic effectiveness of precipitation by increasing erosional resistance through root cohesion [*Gyssels and Poesen*, 2003], whereas trees both reduce the amount of precipitation reaching the ground surface by canopy interception [*Brandt*, 1989] and also provide resistance through root cohesion. If MAP were solely dependent on $\bar{P}$, then increasing MAP would be expected to cause a decrease in hillslope gradient. However, our observations indicate that MAP is weakly positively correlated with mean hillslope gradient in this category. In the central Andes, spatial variability in MAP is strongly controlled by storm duration $\bar{D}$ and frequency $\bar{P}$, in addition to $\bar{P}$ (Figure 4). As a result, spatial variations in topography correlate more strongly with $\bar{P}$ than MAP on the heavily vegetated eastern flanks.

As noted previously, precipitation intensity on the eastern flanks does not vary from north to south in the same manner as the other precipitation metrics. Consequently, the mean hillslope gradient against $\bar{P}$ plot is not separated into distinct groups when data points are classified by latitude (Figure 11a). However, data points that do not fit the overall trend well (hillslope gradients >15° at precipitation intensity > ~40 mm d^{-1}) are all situated north of 17.5°S. In these locations, high precipitation intensity does not drive sufficient erosional efficiency to maintain low hillslope gradients. Three possible reasons for these high hillslope gradients are (1) locally high uplift rates may require steep hillslopes for erosion rates to keep pace with rock uplift, even under high climatic erosional efficiency, (2) the landscape may not be in equilibrium with the local climate and vegetation properties, or (3) precipitation intensity correlates with another property, e.g., temperature, that exerts a greater influence on hillslope gradients. The first hypothesis is consistent with

long-term exhumation rates, which are higher north of 17.5°S [*Horton*, 1999; *Masek et al*., 1994; *McQuarrie et al*., 2008] and may correspond to higher modern uplift rates [*Barnes and Pelletier*, 2006].

4.1.3. Hillslope Gradients in the Central Andes

Precipitation and vegetation characteristics are not able to explain all variability in hillslope gradients. Bedrock lithology can explain some of this variability (Figures 8c, 10a, and 10c), but several additional variables and processes may contribute to spatial variations in hillslope gradient. First, spatial variations in rock uplift require different hillslope gradients to achieve the same erosion rate (Figure 1a). Second, modern topography is unlikely to be in full equilibrium with modern tectonic and/or climatic conditions [*Whipple*, 2001], in which case some variability may be attributed to the landscape undergoing transient adjustments to changing boundary conditions. *Collins and Bras* [2010] argued that the natural landscape is likely to at least partly reflect an equilibrium landscape, because equilibrium states are often approached asymptotically. However, a perturbation in base level can cause a transient wave of incision along a stream. This incision may affect climate-vegetation-hillslope relationships because the response by adjacent hillslopes will tend to persist long after the base level signal has passed. This will lead to a variation in hillslope gradients across the basin where erosion is occurring at different rates (Figure 1e). In this case, mean hillslope gradients would be higher than predicted given the climatic, vegetation, and lithology conditions, even if low gradient, relict topography remains. Finally, only hillslope gradients that are below the local threshold value, an angle limited by the internal strength of the material, can respond to variation in external forcing such as precipitation or uplift rates [*Larsen and Montgomery*, 2012; *Montgomery and Brandon*, 2002; *Schmidt and Montgomery*, 1995]. A large fraction of the domain presented here has a mean hillslope gradient lower than 30° and is therefore likely below threshold hillslope gradients set by the bedrock material. However, where hillslope gradients are at or near their maximum (threshold) value, then relationships with external factors will break down because maximum hillslope gradients are limited by the strength of the underlying material rather than the erosional efficiency or uplift rate [*Larsen and Montgomery*, 2012; *Schmidt and Montgomery*, 1995].

The complete data set suggests that where climatic erosional efficiency is low, and erosion resistance is high, steep hillslopes develop regardless of the uplift rate. Low hillslope gradients are common where erosional resistance is low as a result of either sparse vegetation or weak bedrock lithology. Seasonal, high-intensity precipitation events may also help to maintain high climatic erosional efficiency and low hillslope gradients on the eastern margin of the Andes. Hillslope gradients in the central Andes are therefore controlled by multiple factors, and the dominant factor varies spatially. The observations presented in this study are consistent with vegetation and precipitation exerting an influence on hillslope gradients at the orogen scale.

4.2. Comparison of Results to Simpler Mean Annual Precipitation Analyses

The observations presented in this study provide an extensive data set that helps to elucidate the dominant controls on topography at the scale of a mountain belt. Observations from the Central Andes are consistent with the results of LEM studies in showing that (1) the amount and type of vegetation cover can play an important role in controlling mean hillslope gradients [*Collins et al*., 2004; *Istanbulluoglu and Bras*, 2005] and (2) precipitation intensity and variability can, for fixed erosional resistance, be a strong control on erosional efficiency [*Tucker*, 2004; *Tucker and Bras*, 2000]. Observations from the central Andes also help to identify the dominant processes and forcing factors under different climate conditions and provide quantitative constraints on the transitions between these domains. In the Andes, the transition from dominantly vegetation-controlled to dominantly precipitation-controlled hillslope gradients occurs over a broad range between 1 and 2 m yr^{-1} MAP (Figure 9a). The role of vegetation amount in controlling the spatial variability of geomorphic processes is therefore not restricted to arid, or even subhumid, conditions but is dictated by the amount and type of vegetation, which depends on surface temperature, nutrients, and solar radiation in addition to precipitation.

Montgomery et al. [2001] demonstrated that hemisphere-scale climate gradients exert a first-order control on Andean topography. In their study, erosion potential was evaluated using an erosion intensity metric based on the product of the local slope and the cumulative upslope discharge. At the scale of the Andes, this metric is useful in explaining cross-range asymmetry and large-scale morphology. However, consistent with previous work [*Abrahams*, 1972; *Langbein and Schumm*, 1958; *Melton*, 1957], we have shown that hillslope gradients and precipitation rates are interdependent, through the effects of vegetation cover on the erosional efficiency of the climate. High hillslope gradients may indicate greater erosion potential but may also indicate decreased erosion

efficiency due to high erosion thresholds set by the vegetation cover or bedrock lithology. If changes in precipitation act directly on hillslopes, then the product of precipitation and slope is a good indicator of erosion potential. However, because vegetation can also control hillslope gradients, care must be taken when defining an erosion potential metric such as that used by *Montgomery et al.* [2001]. Furthermore, we have shown that particularly in densely vegetated regions, mean interval between events and precipitation intensity is more robust indicators of high erosion potential than MAP (Figure 10a and equation (3)).

4.3. Caveats to the Analysis and Data Limitations

The precipitation event metrics derived for this study show a spatial pattern that is consistent with modern understanding of central Andean climate [*Garreaud et al.*, 2003]; e.g., high precipitation intensities occur on the north-eastern flanks where strong convective storms occur. However, the data have some limitations. Precipitation rates in the TRMM 3B42v7 data set are instantaneous measurements presented as a discrete 3-hourly time series. Peak precipitation intensities are therefore likely to be underestimated for each event, and therefore, $\overline{P}$ is also likely to be underestimated. Additionally, all individual events therefore have a duration that is a multiple of 3 h and the actual values of mean event duration derived by this method are therefore less meaningful than the spatial distribution of event duration variability. Moreover, some of the shortest, most intense events may not be included. Finally, we assume that precipitation events have a Poisson distribution that can be described entirely by the mean over all events [*Eagleson*, 1978; *Tucker and Bras*, 2000] and do not include a metric for seasonality or temporal clustering of events.

Satellite observations provide precipitation data at a high spatial and temporal resolution and therefore enable new understanding of precipitation variability. However, the time period of observation is still limited; in this study, 11 years of observations are available. The observation period does include both El Niño and La Niña events but may not capture all modern event-scale variability and may be substantially different from earlier climates, e.g., a glacial climate. More importantly, the timescale of change for the variables included in the correlation analysis are significantly different. Our observations cover approximately a decade of climatic variability; vegetation patterns are established over decades, erosion rates vary on multiple timescales, from decadal to millions of years, and topographic features are established over thousand- (small-scale) to million- (orogen-scale) year time periods. The large-scale climate of the central Andes is significantly controlled by the Andean topography and the location in the subtropics [*Garreaud et al.*, 2009; *Lenters and Cook*, 1997], neither of which have changed significantly on thousand-year timescales. However, precipitation and vegetation change on glacial-interglacial timescales and the modern topography may more closely reflect glacial conditions or the cumulative effects of multiple glacial-interglacial cycles [*Tucker and Slingerland*, 1997]. Discrepancies in timescales of response could help to explain some of the variability in the relationships observed in this study.

Due to the spatial resolution of the precipitation data set, all of the variables were averaged over a 0.25° grid. Spatial averaging enables a statistical comparison between all variables, but properties such as vegetation are heterogeneous within a grid cell of this size. Interactions among topography, vegetation, and climate that occur at a smaller scale than the precipitation data set, such as variation of vegetation cover with slope aspect [*Yetemen et al.*, 2010] and valley scale microclimates, are therefore not accounted for in the analysis. The highest resolution data set used in this analysis is the topography. Each 0.25° precipitation grid cell includes ~90,000 DEM grid cells and therefore also include multiple catchments with ridges, river valleys, trunk streams, and hillslopes. Because hillslopes, in comparison to river beds, for example, dominate the landscape, we assume that the mean hillslope gradient in a 0.25° grid cell is representative of the hillslope gradient in that region. Distributions of hillslope gradients from a few sample locations follow a normal distribution (not shown). In addition, the results of an analysis that used the same methodology as presented here but with landscape relief (maximum minus minimum elevation) rather than mean hillslope gradient yielded similar results.

By necessity, the bedrock lithology was classified in fairly broad categories. A higher resolution, more detailed geological data set may reveal further lithologic controls on mean hillslope gradients. Such an analysis would be particularly interesting on the eastern flanks where the bedrock is almost uniformly categorized as "older sediments" and mean hillslope gradient varies greatly. Other studies have shown that threshold hillslope gradients [*Larsen et al.*, 2010] and glacial erosion rates [*Duhnforth et al.*, 2010] depend on spatial variations in rock fracture density. Our observations suggest that in the Andes, maximum hillslope gradients are also limited by the amount of vegetation cover (Figure 8a).

5. Conclusions

We present a new analysis of TRMM precipitation data that quantifies the precipitation event intensity, duration, and frequency in addition to mean annual precipitation. Topographic characteristics of the Central Andes correlate with these precipitation characteristics when considered in combination with vegetation. Where vegetation cover is less than 95%, both MAP and vegetation correlate strongly with mean hillslope gradients on the Andean flanks ($r_{MAP} = 0.6$ and $r_{\%veg} = 0.69$). Multiple interpretations of the observed statistical relationships exist. However, we consider the spatial relationships among vegetation, precipitation, and topography to be consistent with the conclusion that vegetation cover modulates hillslope gradients at the orogen scale. As vegetation cover increases, resistance to erosion increases (Figure 1d) and hillslope gradients increase. However, in the central Andes, MAP can be considered a key underlying driving factor because vegetation is strongly dependent on MAP.

In contrast, where vegetation cover is dense (>95%), elevation ($r = 0.74$), precipitation intensity ($r = -0.56$), and interval ($r = -0.69$) are stronger predictors of mean hillslope gradient than MAP ($r = 0.34$). At high elevations, deep channel incision generates high interfluve relief on erosion resistant, stable hillslopes. At lower elevations, high mean precipitation intensity facilitates high erosional efficiency, resulting in lower mean hillslope gradients (hillslope gradients decrease by ~0.5°/(mm d^{-1})). Greater seasonality and/or less frequent events also correlate with lower hillslope gradients. Spatial variation in rock-uplift rates and bedrock lithology also affect mean hillslope gradients (Figure 1).

When assessing climate-topography interactions, the relevant precipitation metric is therefore dependent on the vegetation cover. In the seasonal, wet climate of the central Andes, the transition between the two regimes occurs between 1 and 2 m yr^{-1} MAP but may differ in other climates depending on the composition of the local plant community. Mean annual precipitation may be a sufficient means of characterizing climatic erosional efficiency but only where $\overline{P}$ is low, vegetation cover is not saturated, and precipitation is the dominant factor determining vegetation cover. In cases where these conditions are not met, precipitation intensity and frequency may better describe erosional efficiency.

Acknowledgments

The data cited in this manuscript are publicly available and can be accessed from the following repositories: (1) Elevation data are available at EOSDIS (NASA's Earth Observing System; Data and Information System); data set name: NASA Shuttle Radar Topography Mission Global 3 arc second number V003. (2) Precipitation data are available from the Mirador portal of GES DISC (Goddard Earth Sciences and Information Services Center); data set name: 3B42: 3-Hour 0.25 × 0.25 degree merged TRMM and other satellite estimates (version 7). (3) Vegetation data were accessed from CIRES Global Land Model Dataset Download Facility; data set name: clm3pftcurrentdayW090_S030.nc. (4) Glaciation data are available from Elsevier's online repository: http://book-site.elsevier.com/9780444534477. (5) Lithological data can be accessed from the USGS Energy Resources Program. Derived data supporting Figures 2 and 4–11 are available as supporting information in Tables S4–S8. This work was funded by grants to T.A.E. and C.J.P. from the US National Science Foundation (EAR awards 0738822 and 0907817). M.L.J. was also supported by a Fellowship from the German DAAD. We thank A. Steiner for useful discussions regarding precipitation analysis. Nicole Gaspirini and three anonymous reviewers provided thorough and thoughtful reviews that helped to improve the manuscript.

References

Aalto, R., T. Dunne, and J. L. Guyot (2006), Geomorphic controls on Andean denudation rates, *J. Geol.*, *114*(1), 85–99, doi:10.1086/498101.

Abrahams, A. D. (1972), Drainage densities and sediment yields in eastern Australia, *Aust. Geogr. Stud.*, *10*(1), 19–41, doi:10.1111/j.1467-8470.1972.tb00127.x.

Abrahams, A. D., and J. J. Ponczynski (1984), Drainage density in relationship to precipitation intensity in the USA, *J. Hydrol.*, *75*(1–4), 383–388, doi:10.1016/0022-1694(84)90061-1.

Allmendinger, R. W., T. E. Jordan, S. M. Kay, and B. L. Isacks (1997), The evolution of the Altiplano-Puna plateau of the Central Andes, *Annu. Rev. Earth Planet. Sci.*, *25*, 139–174, doi:10.1146/annurev.earth.25.1.139.

Barnes, J. B., and J. D. Pelletier (2006), Latitudinal variation of denudation in the evolution of the Bolivian Andes, *Am. J. Sci.*, *306*(1), 1–31, doi:10.2475/ajs.306.1.1.

Barnes, J. B., and T. A. Ehlers (2009), End member models for Andean Plateau uplift, *Earth Sci. Rev.*, *97*(1–4), 105–132, doi:10.1016/j.earscirev.2009.08.003.

Bookhagen, B., and M. R. Strecker (2008), Orographic barriers, high-resolution TRMM rainfall, and relief variations along the eastern Andes, *Geophys. Res. Lett.*, *35*, L06403, doi:10.1029/2007GL032011.

Bookhagen, B., and M. R. Strecker (2012), Spatiotemporal trends in erosion rates across a pronounced rainfall gradient: Examples from the southern Central Andes, *Earth Planet. Sci. Lett.*, *327–328*, 97–110, doi:10.1016/j.epsl.2012.02.005.

Brandt, C. J. (1989), The size distribution of throughfall drops under vegetation canopies, *Catena*, *16*(4–5), 507–524, doi:10.1016/0341-8162(89)90032-5.

Campetella, C. M., and C. S. Vera (2002), The influence of the Andes mountains on the South American low-level, *Geophys. Res. Lett.*, *29*(17), 1826, doi:10.1029/2002GL015451.

Carretier, S., et al. (2013), Slope and climate variability control of erosion in the Andes of Central Chile, *Geology*, *41*(2), 195–198, doi:10.1130/G33735.1.

Champagnac, J.-D., P. Molnar, C. Sue, and F. Herman (2012), Tectonics, climate, and mountain topography, *J. Geophys. Res.*, *117*, B02403, doi:10.1029/2011JB008348.

Chorley, R. J., and M. A. Morgan (1962), Comparison of morphometric features, Unaka mountains, Tennessee and North Carolina, and Dartmoor, England, *Geol. Soc. Am. Bull.*, *73*(1), 17–34, doi:10.1130/0016-7606(1962)73[17:COMFUM]2.0.CO;2.

Churkina, G., and S. W. Running (1998), Contrasting climatic controls on the estimated productivity of global terrestrial biomes, *Ecosystems*, *1*(2), 206–215, doi:10.1007/s100219900016.

Collins, D. B., and R. L. Bras (2010), Climatic and ecological controls of equilibrium drainage density, relief, and channel concavity in dry lands, *Water Resour. Res.*, *46*, W04508, doi:10.1029/2009WR008615.

Collins, D. B., R. L. Bras, and G. E. Tucker (2004), Modeling the effects of vegetation-erosion coupling on landscape evolution, *J. Geophys. Res.*, *109*, F03004, doi:10.1029/2003JF000028.

Cotton, C. A. (1964), The control of drainage density, *N. Z. J. Geol. Geophys.*, *7*(2), 348–352, doi:10.1080/00288306.1964.10420180.

Crozier, M. J. (1999), Prediction of rainfall-triggered landslides: A test of the antecedent water status model, *Earth Surf. Processes Landforms*, *24*, 825–833, doi:10.1002/(SICI)1096-9837(199908)24:9<825::AID-ESP14>3.3.CO;2-D.

Dadson, S., et al. (2003), Links between erosion, runoff variability and seismicity in the Taiwan orogen, *Nature*, *426*, 648–699, doi:10.1038/nature02150.

Daniel, J. R. K. (1981), Drainage density as an index of climatic geomorphology, *J. Hydrol.*, *50*(1–3), 147–154, doi:10.1016/0022-1694(81)90065-2.

DiBiase, R. A., A. J. Heimsath, and K. X. Whipple (2012), Hillslope response to tectonic forcing in threshold landscapes, *Earth Surf. Processes Landforms*, *37*, 855–865, doi:10.1002/esp.3205.

Dietrich, W. E., C. J. Wilson, D. R. Montgomery, J. McKean, and R. Bauer (1992), Erosion thresholds and land surface morphology, *Geology*, *20*, 675–679, doi:10.1130/0091-7613(1992)020<0675:ETALSM>2.3.CO;2.

Duhnforth, M., R. S. Anderson, D. Ward, and G. M. Stock (2010), Bedrock fracture control of glacial erosion processes and rates, *Geology*, *38*(5), 423–426, doi:10.1130/G30576.1.

Eagleson, P. S. (1978), Climate, soil, and vegetation: 2. The distribution of annual precipitation derived from observed storm sequences, *Water Resour. Res.*, *14*(5), 713–721, doi:10.1029/WR014i005p00713.

Ehlers, J., P. L. Gibbard, and P. D. Hughes (Eds.) (2011), *Quaternary Glaciations—Extent and Chronolgy: A Closer Look*, Elsevier Science and Technology Books, San Diego.

Farias, M., R. Charrier, D. Comte, J. Martinod, and G. Herail (2005), Late Cenozoic deformation and uplift of the western flank of the Altiplano: Evidence from the depositional, tectonic, and geomorphologic evolution and shallow seismic activity (northern Chile at 19°30′S), *Tectonics*, *24*, TC4001, doi:10.1029/2004TC001667.

Farr, T. G., et al. (2007), The Shuttle Radar Topography Mission, *Rev. Geophys.*, *45*, RG2004, doi:10.1029/2005RG000183.

Gabet, E. J., D. W. Burbank, J. K. Putkonen, B. A. Pratt-Sitaula, and T. Ojha (2004), Rainfall thresholds for landsliding in the Himalayas of Nepal, *Geomorphology*, *63*(3–4), 131–143, doi:10.1016/j.geomorph.2004.03.011.

Garreaud, R. D., M. Vuille, R. Compagnucci, and J. Marengo (2009), Present-day South American climate, *Palaeogeogr. Palaeoclimatol. Palaeoecol.*, *281*(3–4), 180–195, doi:10.1016/j.palaeo.2007.10.032.

Gyssels, G., and J. Poesen (2003), The importance of plant root characteristics in controlling concentrated flow erosion rates, *Earth Surf. Processes Landforms*, *28*, 371–384, doi:10.1002/esp.447.

Hales, T. C., C. R. Ford, T. Hwang, J. M. Vose, and L. E. Band (2009), Topographic and ecologic controls on root reinforcement, *J. Geophys. Res.*, *114*, F03013, doi:10.1029/2008JF001168.

Horton, B. K. (1999), Erosional control on the geometry and kinematics of thrust belt development in the central Andes, *Tectonics*, *18*(6), 1292–1304, doi:10.1029/1999TC900051.

Houston, J., and A. J. Hartley (2003), The central Andean west-slope rainshadow and its potential contribution to the origin of hyper-aridity in the Atacama desert, *Int. J. Climatol.*, *23*(12), 1453–1464, doi:10.1002/joc.938.

Huffman, G. J., R. F. Adler, D. T. Bolvin, G. Gu, E. J. Nelkin, K. P. Bowman, Y. Hong, E. F. Stocker, and D. B. Wolff (2007), The TRMM multisatellite precipitation analysis (TMPA): Quasi-global, multiyear, combined-sensor precipitation estimates at fine scales, *J. Hydrometeorol.*, *8*, 38–55, doi:10.1175/JHM560.1.

Hulme, M. (1992), A 1951-80 global land precipitation climatology for the evaluation of general circulation models, *Clim. Dyn.*, *7*(2), 57–72, doi:10.1007/BF00209609.

Insel, N., C. J. Poulsen, and T. A. Ehlers (2010a), Influence of the Andes Mountains on South American moisture transport, convection, and precipitation, *Clim. Dyn.*, *35*(7–8), 1477–1492, doi:10.1007/s00382-009-0637-1.

Insel, N., T. A. Ehlers, M. Schaller, J. B. Barnes, S. Tawackoli, and C. J. Poulsen (2010b), Spatial and temporal variability in denudation across the Bolivian Andes from multiple geochronometers, *Geomorphology*, *122*(1–2), 65–77, doi:10.1016/j.geomorph.2010.05.014.

Isacks, B. L. (1988), Uplift of the central Andean plateau and bending of the Bolivian orocline, *J. Geophys. Res.*, *93*(B4), 3211–3231, doi:10.1029/JB093iB04p03211.

Istanbulluoglu, E., and R. L. Bras (2005), Vegetation-modulated landscape evolution: Effects of vegetation on landscape processes, drainage density, and topography, *J. Geophys. Res.*, *110*, F02012, doi:10.1029/2004JF000249.

Jeffery, M. L., C. J. Poulsen, and T. A. Ehlers (2012), Impacts of Cenozoic global cooling, surface uplift, and an inland seaway on South American paleoclimate and precipitation $\delta^{18}O$, *Geol. Soc. Am. Bull.*, *124*(3–4), 335–351, doi:10.1130/B30467.1.

Jeffery, M. L., T. A. Ehlers, B. J. Yanites, and C. J. Poulsen (2013), Quantifying the role of paleoclimate and Andean Plateau uplift on river incision, *J. Geophys. Res. Earth Surf.*, *118*, 852–871, doi:10.1002/jgrf.20055.

Kutzbach, J. E., P. J. Guetter, W. F. Ruddiman, and W. L. Prell (1989), Sensitivity of climate to late Cenozoic uplift in southern Asia and the American west: Numerical experiments, *J. Geophys. Res.*, *94*(D15), 18,393–18,407, doi:10.1029/JD094iD15p18393.

Lague, D., N. Hovius, and P. Davy (2005), Discharge, discharge variability, and the bedrock channel profile, *J. Geophys. Res.*, *110*, F04006, doi:10.1029/2004JF000259.

Langbein, W. B., and S. A. Schumm (1958), Yield of sediment in relation to mean annual precipitation, *Trans. Am. Geophys. Union*, *39*(6), 1076–1084.

Larsen, I. J., and D. R. Montgomery (2012), Landslide erosion coupled to tectonics and river incision, *Nat. Geosci.*, *5*, 468–473, doi:10.1038/ngeo1479.

Larsen, I. J., D. R. Montgomery, and O. Korup (2010), Landslide erosion controlled by hillslope material, *Nat. Geosci.*, *3*, 247–251, doi:10.1038/ngeo776.

Lawrence, P. J., and T. N. Chase (2007), Representing a new MODIS consistent land surface in the Community Land Model (CLM 3.0), *J. Geophys. Res.*, *112*, G01023, doi:10.1029/2006JG000168.

Lenters, J. D., and K. H. Cook (1997), On the origin of the Bolivian high and related circulation features of the South American climate, *J. Atmos. Sci.*, *54*(5), 656–677, doi:10.1175/1520-0469(1997)054<0656:otootb>2.0.co;2.

Masek, J. G., B. L. Isacks, T. L. Gubbels, and E. J. Fielding (1994), Erosion and tectonics at the margins of continental plateaus, *J. Geophys. Res.*, *99*(B7), 13,941–13,956, doi:10.1029/94JB00461.

McQuarrie, N., T. A. Ehlers, J. B. Barnes, and B. Meade (2008), Temporal variation in climate and tectonic coupling in the central Andes, *Geology*, *36*(12), 999–1002, doi:10.1130/g25124a.1.

Melton, M. A. (1957), *An Analysis of the Relations Among Elements of Climate, Surface Properties and Geomorphology*, *Tech. Rep.*, Dept. of Geology, Columbia University, New York.

Molnar, P., R. S. Anderson, G. Kier, and J. Rose (2006), Relationships among probability distributions of stream discharges in floods, climate, bed load transport, and river incision, *J. Geophys. Res.*, *111*, F02001, doi:10.1029/2005JF000310.

Montgomery, D. R., and W. E. Dietrich (1992), Channel initiation and the problem of landscape scale, *Science*, *255*(5046), 926–830, doi:10.1126/science.255.5046.826.

Montgomery, D. R., and M. T. Brandon (2002), Topographic controls on erosion rates in tectonically active mountain ranges, *Earth Planet. Sci. Lett.*, *201*(3–4), 481–489, doi:10.1016/s0012-821x(02)00725-2.

Montgomery, D. R., G. Balco, and S. D. Willett (2001), Climate, tectonics, and the morphology of the Andes, *Geology*, *29*(7), 579–582, doi:10.1130/0091-7613(2001)029<0579:CTATMO>2.0.CO;2.

Musgrave, G. W. (1947), The quantitative evaluation of factors in soil water erosion—A first approximation, *J. Soil Water Conserv.*, *2*, 133–138.

Owen, J. J., R. Amundson, W. E. Dietrich, K. Nishiizumi, B. Sutter, and G. Chong (2010), The sensitivity of hillslope bedrock erosion to precipitation, *Earth Surf. Processes Landforms*, *36*(1), 117–135, doi:10.1002/esp.2083.

Riebe, C. S., J. W. Kirchner, D. E. Granger, and R. C. Finkel (2001), Minimal climatic control on erosion rates in the Sierra Nevada, California, *Geology*, *29*(5), 447–450, doi:10.1130/0091-7613(2001)029<0447:MCCOER>2.0.CO;2.

Roering, J. J., K. M. Schmidt, J. D. Stock, W. E. Dietrich, and D. R. Montgomery (2003), Shallow landsliding, root reinforcement, and the spatial distribution of trees in the Oregon Coast Range, *Can. Geotech. J.*, *40*(2), 237–253, doi:10.1139/t02-113.

Rutllant, J. A., H. Fuenzalida, and P. Aceituno (2003), Climate dynamics along the arid northern coast of Chile: The 1997–1998 Dinámica del Clima de la Región de Antofagasta (DICLIMA) experiment, *J. Geophys. Res.*, *108*, D17, 4538, doi:10.1029/2002JD003357.

Safran, E. B., P. R. Bierman, R. Aalto, T. Dunne, K. X. Whipple, and M. Caffee (2005), Erosion rates driven by channel network incision in the Bolivian Andes, *Earth Surf. Processes Landforms*, *30*, 1007–1024, doi:10.1002/esp.1259.

Schenk, C. J., R. J. Viger, and C. P. Anderson (1999), Maps showing geology, oil and gas fields and geologic provinces of the South America region, *U.S. Geol. Surv. Open File Rep., 97-470D*.

Schildgen, T. F., K. V. Hodges, K. X. Whipple, M. S. Pringle, M. van Soest, and K. Cornell (2009), Late Cenozoic structural and tectonic development of the western margin of the central Andean Plateau in southwest Peru, *Tectonics*, *28*, TC4007, doi:10.1029/2008TC002403.

Schmidt, K. H., and D. R. Montgomery (1995), Limits to relief, *Science*, *270*(5236), 617–620, doi:10.1126/science.270.5236.617.

Schmidt, K. H., J. J. Roering, J. D. Stock, W. E. Dietrich, D. R. Montgomery, and T. Schaub (2001), The variability of root cohesion as an influence on shallow landslide susceptibility in the Oregon Coast Range, *Can. Geotech. J.*, *38*(5), 995–1024, doi:10.1139/t01-031.

Tucker, G. E. (2004), Drainage basin sensitivity to tectonic and climatic forcing: Implications of a stochastic model for the role of entrainment and erosion thresholds, *Earth Surf. Processes Landforms*, *29*(2), 185–205, doi:10.1002/esp.1020.

Tucker, G. E., and R. Slingerland (1997), Drainage basin responses to climate change, *Water Resour. Res.*, *33*(8), 2031–2047, doi:10.1029/97WR00409.

Tucker, G. E., and R. L. Bras (2000), A stochastic approach to modeling the role of rainfall variability in drainage basin evolution, *Water Resour. Res.*, *36*(7), 1953–1964, doi:10.1029/2000WR900065.

Wainwright, J., A. J. Parsons, and A. D. Abrahams (2000), Plot-scale studies of vegetation, overland flow and erosion interactions: Case studies from Arizona and New Mexico, *Hydrol. Processes*, *14*(16–17), 2921–2943, doi:10.1002/1099-1085(200011/12)14:16/17<2921::AID-HYP127>3.0.CO;2-7.

Whipple, K. X. (2001), Fluvial landscape response time: How plausible is steady-state denudation?, *Am. J. Sci.*, *301*(4–5), 313–325, doi:10.2475/ajs.301.4-5.313.

Whipple, K. X. (2009), The influence of climate on the tectonic evolution of mountain belts, *Nat. Geosci.*, *2*(2), 97–104, doi:10.1038/ngeo413.

Yetemen, O., E. Istanbulluoglu, and E. R. Vivoni (2010), The implications of geology, soils, and vegetation on landscape morphology: Inferences from semi-arid basins with complex vegetation patterns in Central New Mexico, USA, *Geomorphology*, *116*(3–4), 246–263, doi:10.1016/j.geomorph.2009.11.026.